University of South Florida
Scholar Commons

Graduate Theses and Dissertations   Graduate School

11-8-2004

Numerical Simulation of Thermal Comfort and Contaminant Transport in Air Conditioned Rooms

Son Hong Ho
University of South Florida

Follow this and additional works at: https://scholarcommons.usf.edu/etd

Part of the American Studies Commons

Scholar Commons Citation

Numerical Simulation of Thermal Comfort and Contaminant Transport

in Air Conditioned Rooms

by

Son Hong Ho

A thesis submitted in partial fulfillment
of the requirements for the degree of
Master of Science in Mechanical Engineering
Department of Mechanical Engineering
College of Engineering
University of South Florida

Major Professor: Muhammad Rahman, Ph.D.
Ashok Kumar, Ph.D.
Thomas Eason, Ph.D.

Date of Approval:
November 8, 2004

Keywords: computational fluid dynamics, multi-component flow, relative humidity, ventilation, heat and mass transfer

Table of Contents

List of Tables

List of Figures

iv

v

Numerical Simulation of Thermal Comfort and Contaminant Transport

in Air Conditioned Rooms

Son H. Ho

ABSTRACT

Health care facilities, offices, as well as workshops and other commercial occupancies, require ventilation and air conditioning for thermal comfort and removal of contaminants and other pollutions. A good design of ventilation and air conditioning provides a healthy and comfortable environment for patients, workers, and visitors.

The increasing developments of computational fluid dynamics (CFD) in the recent years have opened the possibilities of low-cost yet effective method for improving HVAC systems in design phase, with less experiment required. This work presents numerical simulations of thermal comfort and contaminant removal for two typical working spaces where these factors are critical: a hospital operating room with various configurations of inlet and outlet arrangements, and an office with two cases of air distribution systems: underfloor and overhead, also with alternative cases. The 2-D simulation approach was employed. Temperature, relative humidity, contaminant concentration, thermal sensation, predicted mean vote (PMV), and contaminant removal factor was computed and used for assessing thermal comfort and contaminant removal characteristics of the office room and operating room. The result shows good agreements with experimental data take from related literature.

Chapter 1

Introduction

1.1 Overview on Simulation of Air Conditioning in Office Buildings

Within the last few years, underfloor air distribution (UFAD) systems have become popular design alternatives to conventional air distribution (CAD) such as overhead air distribution systems for thermal and ventilation control [1, 2]. Underfloor air distribution is of increasing interest to those who own or design office buildings. Some industry-watchers predict that as many as 35 percent of future office buildings will include UFAD systems [3]. In comparison to classic overhead systems that deliver air at low velocities, typical UFAD systems deliver air through floor diffusers with higher supply air velocities [2]. The UFAD systems can have significant impacts on room air stratification and thermal comfort in occupied zone.

Halza [4] introduced the advantages of UFAD system: improved air quality, lower life-cycle costs, as well as overhead system: better comfort, lower capital cost. Woods [1] did a review by literature searching and field investigations to assess the actual performance of UFAD system in real world. He showed that there are gaps in available data: valid and reliable field data are not from a sufficient population of existing facilities to conclude that underfloor system's performance is superior to overhead system; and that designers must be made aware that underfloor as well as overhead system requires

1

more care in design, installation, and operations. He also recommended that objective analysis should be made before choosing an HVAC system. Webster et al. [2] presented a series of full-scale laboratory experiments to determine room air stratification for a variety of design and operating parameters. Fukao et al. [5] carried out comparative field measurements for both systems in an actual large-scale office building. Webster et al. [6] presented a study about a building that operated with an UFAD system. They showed little troubleshooting with the system operation, pointing out the positive aspects of using well-designed UFAD systems. Bauman [7] offered a work presenting a discussion about several advantages shown by the UFAD systems. In the design stage, CFD simulation can play an important role in improving the understanding of any particular system.

The increasing developments of computational fluids dynamics (CFD) in recent years have opened the possibilities of low-cost yet effective method for improving HVAC system in design phase, with less experiment required. One advantage of CFD modeling is that it allows specific entry details of a room that have relevant airflow. CFD models have been used to study indoor air quality (IAQ) problems, pollutant distributions, and performance of HVAC systems (Chow and Fung [8], Emmerich [9], Gadgil et al. [10]). Hirnikel et al. [11] investigated contaminant removal effectiveness of three air distribution systems for a bar/restaurant by using CFD modeling. They showed that directional airflow systems could reduce people's exposure to contaminants.

Thermal comfort can be predicted based on Fanger's PMV model [12], which assumes a uniform thermal environment. Thermal sensation index from Rohles and Nevins' work [13] is also widely used for assessing thermal comfort. Relative humidity can be computed by using the procedure recommended in [14].

2

1.2 Overview on Simulation of Air Conditioning in Hospital Operating Rooms

The main purpose of the HVAC system design for operating rooms is to prevent the risk of infections during surgical operations while maintaining adequate comfort conditions for the patient and surgical staff.   There are standards suggested for air-conditioning systems for operating rooms around the world. The American Institute of Architects (AIA) has guidelines for designing and construction of hospitals and health care facilities in the USA. The institute has presented its latest revision of its guidelines in 2001 [16]. Proper indoor comfort conditions and indoor air quality are prerequisites for securing a safe and suitable environment for operating rooms. Many experimental studies have been presented about infections and related factors in a typical operating room [17, 18]. Lewis [19] studied the influence of room air distribution on infection rate in an operating room. He concluded that optimal air distribution played an important role in environmental conditions within a surgical room.

Memarzadeh [20] proposed a methodology for minimizing contamination risk in hospital rooms. Mora et al. [21] studied thermal comfort in operating rooms. They based their analysis on the thermal comfort model proposed by Fanger [12]. They concluded that the only means to provide thermal comfort for the surgical staff was to eliminate or to minimize the heat transfer from the surgical lights. They realized that more research is needed to evaluate an acceptable thermal environment in operating rooms. It can be observed that there is a need to predict ambient conditions within an operating room.

Numerical analysis is usually employed for simulating airflow and temperature distribution. Memarzadeh and Manning [22] studied the performance of a ventilation system in a typical patient room using CFD modeling. They were able to predict the

3

necessity of using baseboard heating in extreme weather conditions. Hirnikel et al. [11] investigated contaminant removal effectiveness of three air distribution systems for a bar/restaurant by using CFD modeling. They showed that directional airflow systems can reduce people's exposure to contaminants. Memarzadeh and Manning [23] simulated contaminant deposition on an operating room using CFD air flow modeling. They showed that laminar flow conditions were the best choice for ventilation systems when contaminant deposition was considered.

Health care facilities, as well as workshops and other commercial occupancies, require ventilation and air conditioning for thermal comfort and removal of contaminants as well as other pollutions. A good design of ventilation and air conditioning provides a healthy and comfortable environment for people such as patients, workers, and visitors. Poorly ventilated workspaces not only make people feel uncomfortable but also can make them become infected or intoxicated since the likelihood of air borne pathogens or other kinds of toxic chemicals are quite high.

1.3 Thesis Outlines

This thesis presents the CFD simulation of two problems of air-conditioned rooms. Chapter 2 reviewed the relevant details of simulation approach. In Chapter 3, two different air distribution systems for office buildings were compared on thermal comfort and contaminant removal effectiveness. Each system has its own variation, such as inlet location for underfloor system and inlet angle for overhead system. In Chapter 4, an operating room in hospital was modeled, different cases of inlet angle and outlet arrangement were investigated. The simulation results were compared for assessing

4

thermal comfort and contaminant removal characteristics. The CFD computations for all simulations were done on FIDAP (Fluent, Inc.), a finite element analysis CFD software package. The post-processing computations were done on Matlab (The MathWorks, Inc.). The results from the simulations were also compared to experimental data on operating rooms and office rooms, taken from literature.

1.4 Nomenclature

C Mean contaminant concentration, kg of contaminant/kg of air mixture

c_p Specific heat of air, J/(kg.K)

D   Mass diffusivity of species in air, m^2/s

f_{cl} Ratio of clothed surface area to nude surface area

Gr   Grashof number

g   Gravity acceleration, m/s^2

h Heat transfer coefficient, $W/(m^2.K)$

I Thermal resistance, m^2K/W

k Thermal conductivity of air, W/(m.K)

L Characteristic length

m Concentration of species, kg of species/kg of air mixture

M Metabolic heat generation flux, W/m^2 of naked body area

p Pressure; partial pressure (with subscript), Pa

Re   Reynolds number

T Temperature; mean temperature (with subscript), °C

U Characteristic velocity, m/s

5

u	velocity, m/s
v	Mean air speed relative to the body, m/s
W	External work, W/m^2 of naked body area
Y	Thermal sensation index

Greek Symbols

β	Thermal expansion coefficient, 1/K
ϕ	Relative humidity
μ	Viscosity of air, kg/(m.s)
ρ	Density of air, kg/m^3

Subscripts

1	Water vapor
2	Contaminant
a	Air
BZ	Breathing zone
c	Convective
cl	Clothing
E	Exhaust
r	Radiant
ref	Reference
S	Supply
s	Saturated (water vapor)
w	Water vapor

6

Chapter 2

Simulation Approach

2.1 Introduction

To predict the indoor thermal environment, it is necessary to determine air velocity, temperature, and relative humidity in a room. The prediction was carried out by solving coupled equations for the conservation of mass (for the whole air mixture as well as for each species), momentum, and energy. For most air conditioning applications in indoor environment assessing and designing, the solution of interest is steady state.

Since the real problems are three-dimensional (3-D) by nature, using 3-D models to simulate them would be the best approach. However, 3-D simulations require very large amount of computation memory and time, sometimes possibly exceed the available resources. Besides, from the design point of view, it can be very difficult to locate and to assess the key parameters, which most significantly affect the performance of a design, from a 3-D simulation where the interaction of space dimensions complicates the results. Two-dimensional (2-D) simulation requires less computation resources, but still can provide reasonable results on what parameters are important and how they affect the performance of a design. It describes the phenomenon of fluid flow and heat transfer in the local section of interest (e.g. near working people) but not for the entire region. As a basic approach for the problems at hand, this work employed 2-D simulations.

7

The fluid properties are assumed constants. They were taken at the reference temperature, $T_{ref} = 22^{o}C = 295$ K, as follows:

- $\rho = 1.1967$ kg/m^3
- $\mu = 1.8273E\text{-}5$ kg/(m.s)
- $c_p = 1.0043E3$ J/(kg.K)
- $k = 2.5776E\text{-}2$ W/(m.K)
- $\beta = 3.3932E\text{-}3$ K^{-1}
- $D_1 = 2.5448E\text{-}5$ m^2/s
- $D_2 = 2.5033E\text{-}5$ m^2/s

2.2 Governing Equations

Consider a steady state, two-dimensional incompressible flow of air as a multi-component fluid, which includes dry air, water vapor, and contaminant gas. The fluid properties are considered as constants except the varying density for buoyancy term in the momentum equation.

The equation for the conservation of mass applied for the air mixture as a whole or carrying fluid is given by

$$\nabla \cdot \mathbf{u} = 0 \tag{2.1}$$

Assuming that the mass diffusivities of species in air are scalars, thermal diffusion (Soret effect) is negligible, and there is neither source nor chemical reaction, the equations for the mass conservation of water vapor and contaminant gas as carried species are

$$\mathbf{u} \cdot \nabla m_1 = D_1 \nabla^2 m_1 \tag{2.2}$$

8

$$\mathbf{u} \cdot \nabla m_2 = D_2 \nabla^2 m_2 \tag{2.3}$$

The buoyancy force term arising from density variation is included by means of the Boussinesq approximation based on the assumptions that variation in fluid density affect only the buoyancy term and fluid density is a function of temperature and concentration only. For most HVAC applications, the species concentrations are very small such that the dependency of buoyancy term on them can be neglected. The equation for the conservation of linear momentum is given by

$$\rho \mathbf{u} \cdot \nabla \mathbf{u} = -\nabla p + \mu \nabla^2 \mathbf{u} + \rho \mathbf{g} \beta \left(T - T_{ref} \right) \tag{2.4}$$

Assuming that there is no heat generation, thermal conductivity is scalar, energy flux due to inter-diffusion and Dufour effect are negligible, and the equation for the conservation of energy is given by

$$\rho c_p \mathbf{u} \cdot \nabla T = k \nabla^2 T \tag{2.5}$$

The equation Eq. 2.4 is a vector equation for velocity (and pressure). It is actually two coupled scalar equations of two velocity components (and pressure). This equation describes the mixed convection fluid flow, that is both forced convection and natural convection exist. The last term in the right hand side of Eq. 2.4 is the buoyancy term, which represents the effect of natural convection. The buoyancy term couples the equations Eq. 2.4 and 2.5 through temperature variable. If the buoyancy term is small, it can be discarded and thus decoupling the equations except for the convection terms. For judging if the buoyancy effect is small enough to be eliminated without causing significant errors, Reynolds number and Grashof number are used to characterize the effect of forced convection and natural convection, respectively, given by

9

$$Re = \frac{\rho U L}{\mu}$$

$$Gr = \frac{\rho^2 g \beta (T - T_{ref}) L^3}{\mu^2}$$

where U and L are the characteristic velocity and characteristic length, respectively.

If $Gr > Re^2$ then natural convection dominates. If $Gr < Re^2$ then forced convection dominates. If $Gr \ll Re^2$ then the effect of natural convection is very small and the flow can be considered to be forced convection only.

The typical values of the dimensionless numbers for the air-conditioned rooms are $Re \sim 10^4$ and $Gr \sim 10^9$. Then $Gr \sim Re^2$, the effects of forced convection and natural convection are generally the same; the flow is actually mixed convection and a little natural convection dominated. Therefore, the buoyancy term has a very strong effect on the solution and cannot be eliminated.

The solution obtained from solving the equations Eq. 2.1 – 2.5, associated with their boundary conditions, gives six primary parameters: two velocity components, pressure, temperature, water vapor concentration, and contaminant concentration.

2.3 Relative Humidity

From the primary parameters: temperature, water vapor concentration, and pressure, relative humidity can be computed by using the procedure recommended in [14], which is summarized as follows:

$$\phi = \frac{p_w}{p_{ws}} \tag{2.6}$$

where

10

$$p_w = \frac{(101325 + p)m_1}{0.62198 + 0.37802m_1} \tag{2.7}$$

$$p_{ws} = 1000\exp\left[-\frac{5.800 \times 10^3}{T + 273.15} - 5.516 - 4.864 \times 10^{-2}(T + 273.15) + \right.$$
$$+ 4.176 \times 10^{-5}(T + 273.15)^2 - 1.445 \times 10^{-8}(T + 273.15)^3 + \tag{2.8}$$
$$\left. + 6.546\ln(T + 273.15) \right]$$

2.4 Thermal Comfort Assessment

One of the most frequently cited thermal comfort models is the Fanger model. The Fanger model is based on steady-state energy balance. This model was originally developed to predict human thermal comfort in office-like environments and has gained wide usage in the HVAC industry because its simplicity [15]. Predicted mean vote (PMV) is a parameter for assessing thermal comfort in an occupied zone based on the conditions of metabolic rate, clothing, air speed besides temperature and humidity. From the work of Fanger given in [12], the value of PMV is given by

$$\begin{aligned} \text{PMV} = &\{0.303\exp[-0.036(M - W)] + 0.028\}\{(M - W) \\ &- 3.05 \times 10^{-3}[5733 - 6.99(M - W) - p_w] - 0.42[(M - W) - 58.15] \\ &- 1.7 \times 10^{-5}M(5867 - p_w) - 0.0014M(34 - T_a) \\ &- 3.96 \times 10^{-8}f_{cl}\left[(T_{cl} + 273)^4 - (T_a + 273)^4\right] - f_{cl}h_c(T_{cl} - T_a)\} \end{aligned} \tag{2.9}$$

where

$$\begin{aligned} T_{cl} = &35.7 - 0.028(M - W) \\ &- I_{cl}\{3.96 \times 10^{-8}f_{cl}\left[(T_{cl} + 273)^4 - (T_a + 273)^4\right] + f_{cl}h_c(T_{cl} - T_a)\} \end{aligned} \tag{2.10}$$

$$h_c = 2.38(T_{cl} - T_a)^{0.25} \text{ or } h_c = 12.1\text{v}^{0.5}, \text{ whichever is greater} \tag{2.11}$$

$$f_{cl} = \begin{cases} 1.00 + 1.29I_{cl} \text{ for } I_{cl} \leq 0.078\,\text{m}^2\text{K/W} \\ 1.05 + 0.645I_{cl} \text{ for } I_{cl} > 0.078\,\text{m}^2\text{K/W} \end{cases} \tag{2.12}$$

11

Thermal sensation index represents the effect of environmental and personal variables on thermal response and comfort level, such as temperature, humidity, sex, and length of exposure. Thermal sensation can be predicted using empirical equations from the work of Rohles and Nevins given in [13]. The empirical equation for men and women combined with exposure period of 3 hours, conversed for SI units, is given by

$$Y = 0.243T_a + 0.000278p_w - 6.802 \tag{2.13}$$

Thermal sensation index values refer to the thermal sensation scale adopted by ASHRAE now known as the ASHRAE thermal sensation scale. PMV values also refer to this scale. ASHRAE thermal sensation scale ranges from -3 to 3 as follows:

- 3 = hot
- 2 = warm
- 1 = slightly warm
- 0 = neutral
- -1 = slightly cool
- -2 = cool
- -3 = cold

2.5 Contaminant Removal Effectiveness

For assessing the effectiveness of an occupied zone, the contaminant removal effectiveness (CRE) is used. The CRE was determined based on the mean contaminant concentration in the supply inlet, in the exhaust outlet, and in the occupied zone [9].

$$\text{CRE} = \frac{C_E - C_S}{C_{BZ} - C_S} \tag{2.14}$$

12

where C_E is the mean concentration in exhaust; C_S is the mean concentration in supply air and C_{BZ} is the mean concentration in occupied zone. Assuming that the supply airflow is contaminant-free, the contaminant removal effectiveness from (2.14) can be computed as

$$\text{CRE} = \frac{C_E}{C_{BZ}} \tag{2.15}$$

2.6 Computation Procedures

The simulations were done on CFD software package FIDAP (Fluent, Inc.). For each simulation, two steps were performed. First, the strongly coupled problem of the equations Eq. 2.1, 2.4, and 2.5 was solved. Then the advection-diffusion problem of the species equations, Eq. 2.2 and 2.3, was solved with known velocity field from the first step. Source code for the typical cases of the two simulation sets in Chapters 3 and 4 are given in Appendices A and B. The output numerical solution includes velocity component, pressure, temperature, water vapor concentration, and contaminant concentration at every node of the computation region.

In post-processing stage, available commands in FIPOST, the post-processing module in FIDAP package, were used when possible. The average values of speed, temperature, and contaminant concentration were computed directly by using the MEAN command, which is a weighted average based on the size of the elements. Similarly, the average contaminant on the outlet was computed by using the FLUX command.

The relative humidity, which depends on temperature, pressure, and water vapor concentration, can be computed by two methods: (i) using user subroutines written by user and incorporated into FIDAP, and (ii) using Matlab. The first method is very

13

convenient for getting the relative humidity directly from FIDAP as a primary variable, but require the to include the species equation for water vapor in the first step, i.e. solving the equations Eq. 2.1, 2.4, 2.5, and 2.2 simultaneously, which costs more computation resources. The second method, using Matlab, gives a more flexible alternative. The FIDAP numerical solution was exported into neutral files, then read into Matlab. Several Matlab M-file were created to compute relative humidity at every nodes and mean values, as well as other relevant parameters such as thermal sensation index, PMV, CRE. Matlab also handles the 2-D contour and vector plots the variables of interest (velocity, temperature, relative humidity, and contaminant concentration).

14

Chapter 3

Simulation of Underfloor and Overhead Air Distribution Systems in an Office

3.1 Introduction

This study compares thermal environments and contaminant removal effectiveness (CRE) of two air distribution systems for an office setting by the use of computational fluid dynamics (CFD) modeling. The air supply distribution and exhaust arrangement were modeled for an underfloor air distribution (UFAD) system and an overhead air distribution system. The study of a thermally comfortable typical cubicle in a large office floor requires detailed information about distribution of air velocity, air temperature and relative humidity in the indoor environment. The CRE of each system was determined for contaminant distributions. The model included a typical cubicle in a large office floor in a steady-state condition with a chair, a desk with a PC on top, and heat sources such as seated people and lights. For underfloor air distribution system, air entered the occupied zone through an inlet located at floor level supplying a vertical upward inflow. Three different locations of inlet diffuser were considered. For overhead air distribution, the inlet is located on the ceiling with slower and cooler inflow. Three cases of inlet angle were considered. For both systems, the air return location is on the ceiling at the same place. Distributions of velocity, temperature, relative humidity, and contaminant concentration in various cases for both systems were computed. Thermal

15

comfort factors and contaminant removal effectiveness were assessed for the two systems. The results were compared among cases of each system, as well as between two typical cases of the two systems. A comparison with experimental data of an actual office building given in literature was also offered.

The objective of this part of the work is to use CFD modeling to simulate airflow in two air distribution systems: underfloor and overhead, for a single cubicle on an office floor. The results can be related to thermal environment, indoor air quality and ventilation effectiveness. Temperature and relative humidity distributions as well as contaminant concentration and velocity patterns are to be presented. Thermal comfort is predicted based on Fanger's PMV model [12], which assumes a uniform thermal environment. Thermal sensation index from Rohles and Nevins' work [13] is also used for assessing the thermal comfort of the cubicle. The results are to be compared to each other. CFD prediction results are also compared to experimental results reported in [5].

3.2 CFD Model

A cubicle in a large office floor was modeled as a rectangular region. Two air distribution systems were considered in the present investigation: underfloor air distribution (Fig. 3.1) and overhead air distribution (Fig. 3.2). These two figures show a typical set up and essential dimensions of the cubicle. The essential dimensions are denoted in general forms as L1 to L16 for lengths and A1 for angle. Giving the dimensions in general form makes it flexible for further parameterized investigation, as the alternation of essential dimensions can be performed without significant changes in the CFD program. The numerical values of the lengths L1 to L14 used for the

16

computations in this paper are given in Table 3.1 for both systems. The inlet length denoted as L15 is different between two systems (underfloor and overhead) and takes corresponding numerical values from Table 3.2.

For underfloor system (Fig. 3.1), various locations of the inlet diffuser can be considered by altering the length L16. In this paper, three such locations were taken for computation: close to the backside of the seat (typical), under the desk, and facing the outlet. The values of L16 as the inlet location parameter are given in Table 3.2.
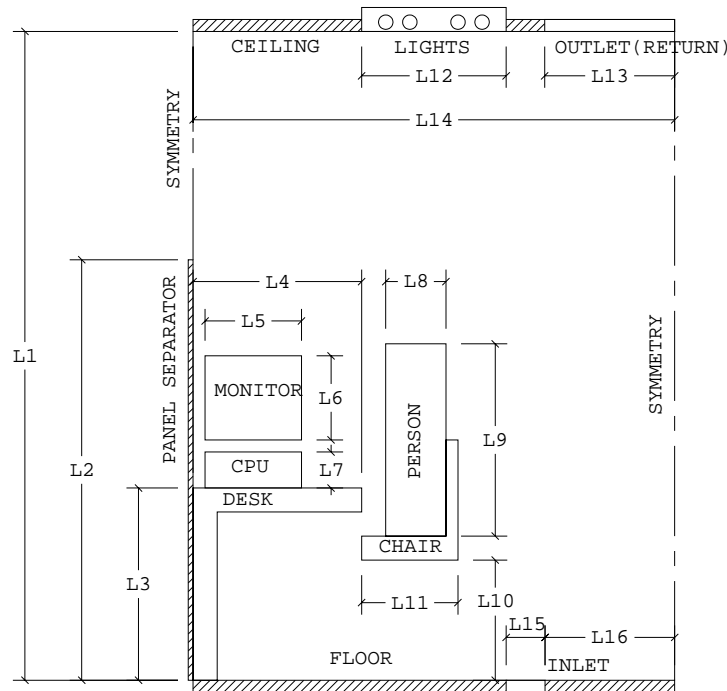
Figure 3.1 Model of Office Cubicle with Underfloor Air Distribution System

For overhead system (Fig. 3.2), although the location of the inlet diffuser remains unchanged, various inlet angles can be considered by setting the angle A1. The inlet angle is measured downward from the ceiling. For this paper, three inlet angles were

17

taken: 30 (typical), 45, and 60 degrees. The numerical values A1 corresponding to each

simulation case are given in Table 3.2 as well.
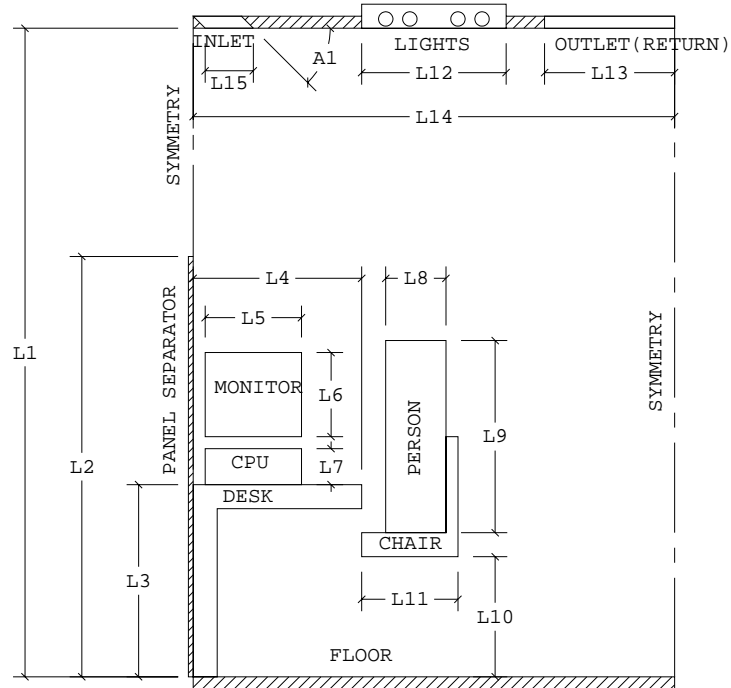
Figure 3.2 Model of Office Cubicle with Overhead Air Distribution System

The office floor layout can be thought of as including many aisles of cubicles.

Each block of an aisle includes two cubicles symmetrically facing each other through a

panel separator between them. The left boundary above the separator is considered as

symmetry boundary. The open space on the right side models half of the walkway

(perpendicular to paper's plane) between cubicle aisles. The right boundary was also

taken as symmetry boundary because of the symmetric of floor layout. Right next to the

separator is a desk and a personal computer (CPU and monitor) placed on it. A person is

sitting on a chair, facing the computer. The lights are located on the ceiling, right above

18

the person's position. On the backside of the person is the right symmetry boundary at half of the walkway. The air return outlet is placed on the ceiling above that region for both cases. The top face of the monitor was defined in CFD model as the entity "hot top" for releasing heat flux to the surrounding. There was also heat flux from the lights. The person was considered as constant temperature surface and also imposed a flux of water vapor. Contaminant gas as evaporating cleaning chemicals released from the rug on the floor, as a mass flux.

Table 3.1 Dimension Parameters on Figures 3.1 and 3.2, meter(s)

L1	L2	L3	L4	L5	L6	L7	L8	L9	L10	L11	L12	L13	L14
2.7	1.75	0.8	0.7	0.4	0.35	0.15	0.25	0.8	0.5	0.4	0.6	0.54	2.0

Table 3.2 Inlet Boundary Conditions, Inlet Setup and Simulation Cases

Air distribution system	Underfloor			Overhead		
Inlet temperature	$20^{o}C$			$18^{o}C$		
Inlet speed	1.0 m/s			0.6 m/s		
Inlet direction	Vertical upward			Oblique downward		
Inlet width (L15)	0.16 m			0.2 m		
Varying parameter	Inlet location, L16			Inlet angle, A1		
	0.54 m Typical	1.54 m Under desk	0.18 m Face outlet	30° Typical	45° -	60° -
Simulation case number	1	2	3	4	5	6

19

The two models are almost identical except for the air supply inlet. Key differences between the systems arise with the location and the size (and thus the flow rate) of inlets. For the underfloor system, the inlet is located near the back of the person on the floor, which is the typical setup. Two more locations of inlet were considered: under the desk and facing the outlet, which make two limit locations. For the overhead system, the supply diffuser is located on the ceiling, right above the separator, symmetrically sharing for two opposite cubicles; hence our model on Fig. 3.2 takes a half of the diffuser size as its inlet size. The typical inlet angle is 30 degrees. By exploring how inlet angle affects thermal comfort and contaminant removal characteristics of the model, two more inlet angles were considered: 45 and 60 degrees.

Because the air is supplied directly into the occupied zone in the underfloor system, supply air temperatures can be higher than that used for conventional overhead system. Higher supply air temperatures would suggest that higher supply air velocities are required. Inlet speed and temperature for each system are given in Table 3.2.

The CFD simulations estimated variables such as pressure, velocity, temperature, and contaminant concentration for each cell, throughout the entire cubicle in accordance with mass and concentration conservation equations. Six simulations were performed, three for the underfloor system and the other three for the overhead system. The simulation cases and associated inlet boundary conditions are given in Table 3.2. Details of boundary conditions are given in Table 3.3.

For each simulation, velocity components and temperature were found first by solving the coupled equations Eq. 2.1, 2.4, and 2.5, then the species concentrations were solved from the equations Eq. 2.2 and 2.3 with known velocity field.

20

Table 3.3 Boundary Conditions for Office Room Simulation

No.	Entity	Velocity	Temperature/ Heat flux	Water vapor concentration	Contaminant concentration
1	Inlet	See Table 3.1	See Table 3.1	0.011 kg/kg air	0 kg/kg air
2	Symmetry	$UX = 0$	Flux =0	Flux = 0	Flux = 0
3	Hot top	0	Flux = 100 W/m^2	Flux = 0	Flux = 0
4	Lights	0	Flux = 75 W/m^2	Flux = 0	Flux = 0
5	Person	0	Temp = 33°C	Flux = 5E-7 kg/(m^2.s)	Flux = 0
6	Floor	0	Flux = 0	Flux = 0	Flux = 1E-6 kg/(m^2.s)
7	Outlet	Unknown	Unknown	Unknown	Unknown
8	Others	0	Flux = 0	Flux = 0	Flux = 0

3.3 Results and Discussion

Three cases were simulated for the underfloor system (simulations 1, 2, and 3) and another three for the overhead system (simulations 4, 5, and 6). For each simulation, the governing equations Eq. 2.1 – 2.5, associated with the boundary conditions given in Tables 3.2 and 3.3, were solved by using finite element analysis. Each solution included velocity field, pressure, temperature, water vapor concentration, and contaminant concentration. Relative humidity distribution was then computed by using equations Eq. 2.6 – 2.8. Predicted mean vote (PMV) was calculated based on solution average values using equations Eq. 2.9 – 2.12. Thermal sensation index was calculated from equation Eq. 2.13 and contaminant removal effectiveness, equation Eq. 2.15.

21

Figure 3.3 shows velocity distribution for typical case of underfloor system (simulation 1). The velocity vector field was plotted on color background showing speed distribution. The cool airflow entered the cubicle vertically through a floor-level diffuser at uniform full speed (1.0 m/s). The main flow slightly bent to the left then vertically swept along the local space near the person's back, up to about 1.8 m height, spread and bent to the right toward the return outlet at reducing speed. Near the outlet, a fraction of the main flow did not go through the outlet but made a sharp U-turn and vertically went down along the symmetry boundary. The upward flow were dominated by forced convection from the imposed inlet velocity and also induced by natural convection due to higher temperature surface along the person's back, while the downward flow was under the effect of natural convection only because of its lower temperature. The upward and downward flow created a region of circulation near the backside of the person (right hand side on Fig. 3.3).
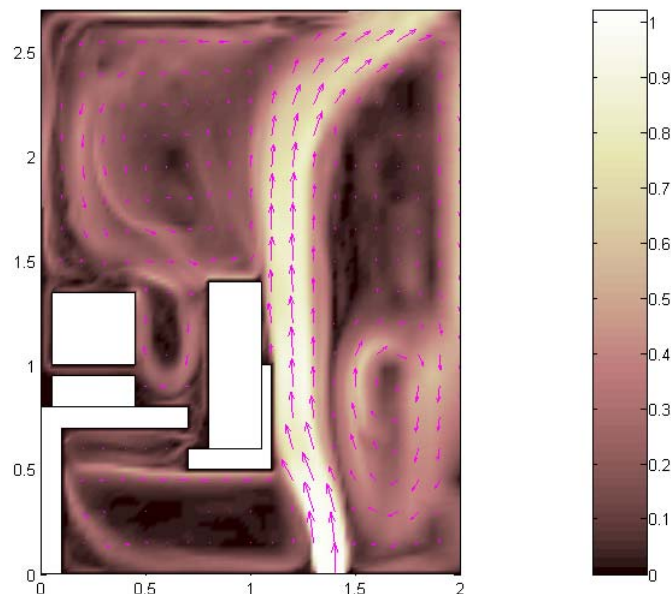
Figure 3.3 Velocity Field for Simulation 1, m/s

22

There was also a small flow separated from the main flow, sweeping under the chair and the desk, creating some kind of air mixing flow, and moving up through the gap between the person and the desk. This small flow might have some positive but little effect on the natural convection flow along the front surface of the person, which caused a slight circulation in the region between the person and the computer. The region above the person and the computer was a mixing zone mostly caused by natural convection, showing unclear gentle circulations.

Figure 3.4 shows the temperature distribution for typical underfloor case. The right hand side region, or backside of the person, was a zone with temperature as low as inlet air temperature, since the backside circulation caused by the main stream was strong that make the air in that region well mixed with the cool air from inlet, inducing heat transfer, mostly by convection.
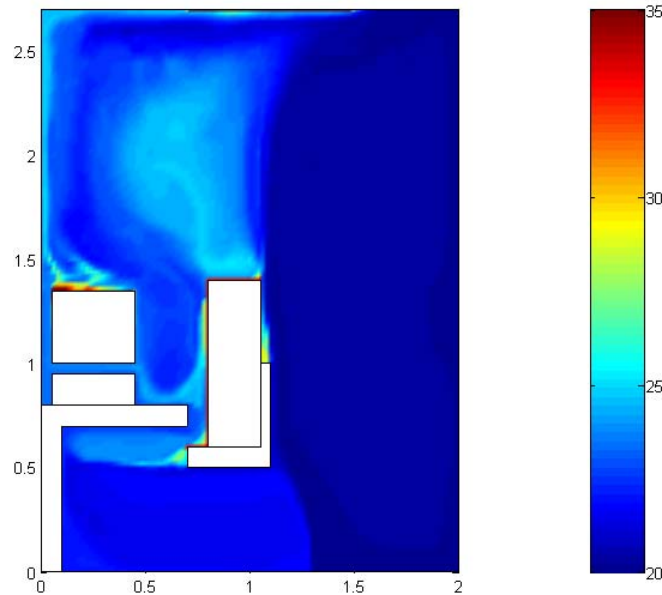
Figure 3.4 Temperature Distribution for Simulation 1, ^{o}C

23

On Fig. 3.4, in other regions outside the main stream, temperature was higher but still fair-manner distributed due to both diffusion and natural convection. Slight circulation under the chair and the desk as well as the absence of heated surface kept the region colder than the working space above where there are hot surfaces such as the person, the computer, and the lights. There were small moderate temperature zones around the person model, which was of constant temperature, and high temperature zones close to the computer top and lights where there were heat fluxes coming into the occupied zone. A warmer region of about $25^{\circ}C$ was formed in the region above the person.

Figure 3.5 is the plot of relative humidity distribution for typical underfloor case. Relative humidity is a function of absolute pressure, water vapor concentration, and temperature. Since the gage pressure in the whole region was found very small (at the order of 1 Pa) compared to the atmospheric pressure (at the order of 101 kPa), it does not affect the total absolute pressure significantly. The water vapor concentration also does not change much, since the only water vapor supply was the person's surface with very small flux. Therefore, the relative humidity distribution was mostly dependent on temperature distribution, and their plots appear similar. In the backside circulation zone, it is observed a uniform distribution at about 75%. In the person's working zone, relative humidity was about 50%-65% everywhere and higher at hot surfaces, such as computer top, and lights. Around the person area, relative humidity was between 50% and 60%; a zone of low relative humidity (around 50%) was found in front of the person and in the warmer region above.

24
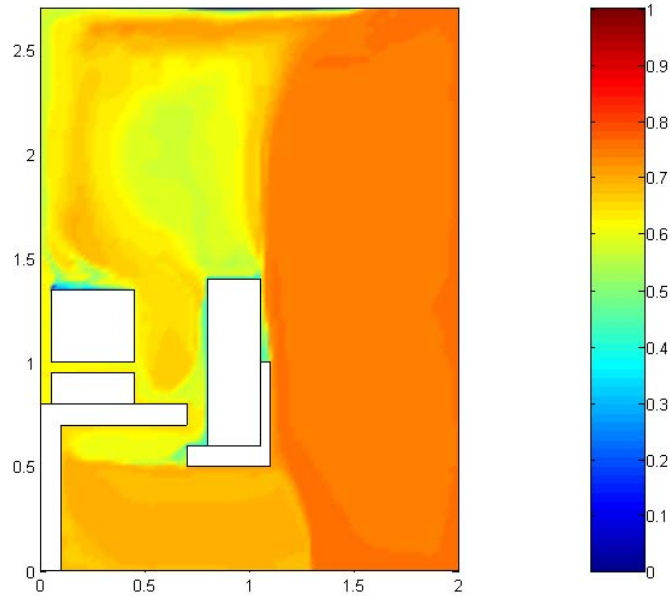
Figure 3.5 Relative Humidity Distribution for Simulation 1

Figure 3.6 shows the distribution of contaminant concentration for typical underfloor system. In this CFD models, it is supposed that contaminant to be releasing from the floor as a constant flux. Contaminant transport was driven by concentration gradient and by convection. On Fig. 3.6, it can be seen that there is almost zero contaminant concentration in the main flow and regions next to it, since the inlet flow of fresh air swept through the region and brought the contaminant to the outlet by convection. The region around, above and in front of the person was almost contaminant free, by the effects of the small flow through the gap and the natural convection flow along the front surface. The backside circulation, while sweeping along the floor, kept the high contaminant concentration confined in the small zone right above the floor. Under the desk and the chair, air was moving very slowly, thus the main transport mean was by diffusion that made a uniform-like distribution of higher concentration under the desk.

25
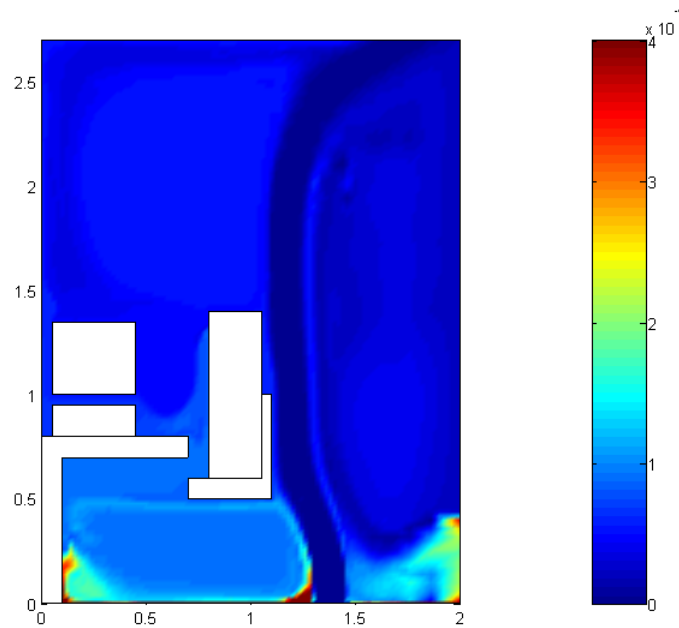
Figure 3.6 Contaminant Concentration Distribution for Simulation 1, kg/kg air

The results from the simulations 2 and 3 show some different behavior of the airflow with respect to different inlet locations. We will comment on their affects on average parameters controlling thermal comfort and contaminant removal.

For a convenient view of how thermal environment and contaminant concentration respond to an air distribution system, we consider the vertical distributions of air speed, temperature, relative humidity, and contaminant concentration. At each different height, average values of the parameter of interest were taken over all the width of the region. Figure 3.7 presents a comparison of vertical distribution of average air speed for three cases of the underfloor system. The typical case shows a moderate vertical distribution of air speed in the range of 0.2-0.3 m/s, while the under-desk-inlet case (simulation 2) and the inlet-facing-outlet case (simulation 3) show significant changes of air speed to the height. Both cases give high air speed as high as 0.4 m/s at

26

about 1.7 m, right on top the person, which might not comfortable for the person. For the under-desk-inlet case, the air speed was higher than that for typical case in the region under the desk and the chair, as one might expect, which is not comfortable as well. The average air speed in that region was far higher for the case of inlet facing outlet, but most of the high air speed concentrated at the inlet region as it was coupled with the outlet to form a straight open flow channel, which does not much affect the person.
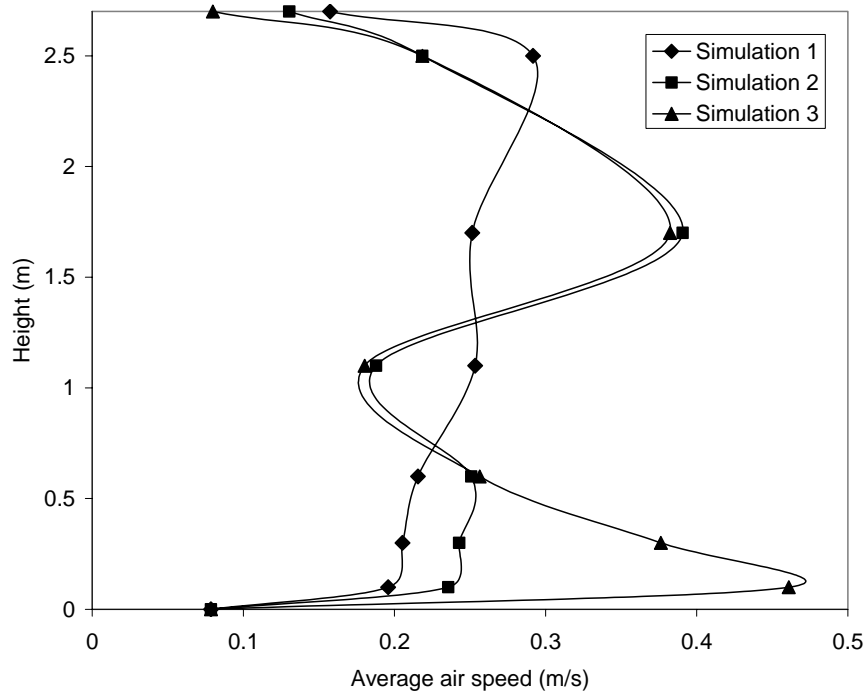
Figure 3.7 Vertical Distribution of Average Air Speed for Underfloor System

Figure 3.8 shows the vertical distribution of temperature for underfloor cases. All the three cases show similar distributions. Temperature was higher for typical case along most of the sitting height of the person but lower at height closer to the ceiling. Vertical average temperature was most uniform in under-desk-inlet case with a narrow band of

27

temperature variation of 20°C-23°C. The temperature in the region under the desk and chair is important for comfort of the lower part of the person such as legs and feet. Typical case shows the best characteristics in this aspect while the other cases might cause the "cold feet" effect on the person.
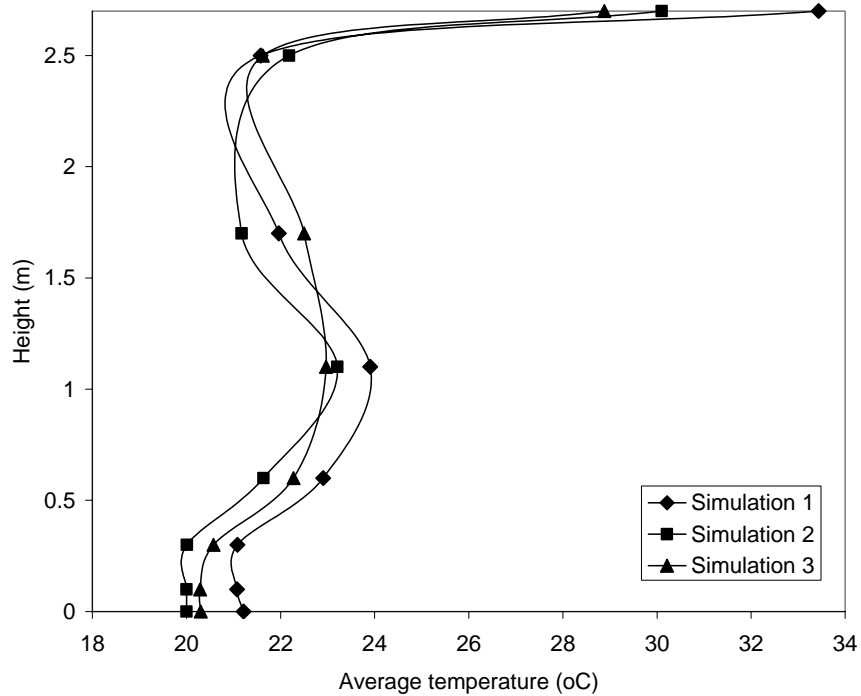
Figure 3.8 Vertical Distribution of Average Temperature for Underfloor System

Figure 3.9 shows the vertical distribution of average relative humidity for three underfloor cases. The typical case had the most uniform distribution and provided best comfort for the lower region, ranging in 63%-72%. The under-desk-inlet case shows more uniform relative humidity in the heights occupied by the person but the higher in the lower region and lower in higher region made the over all performance less satisfied.

28
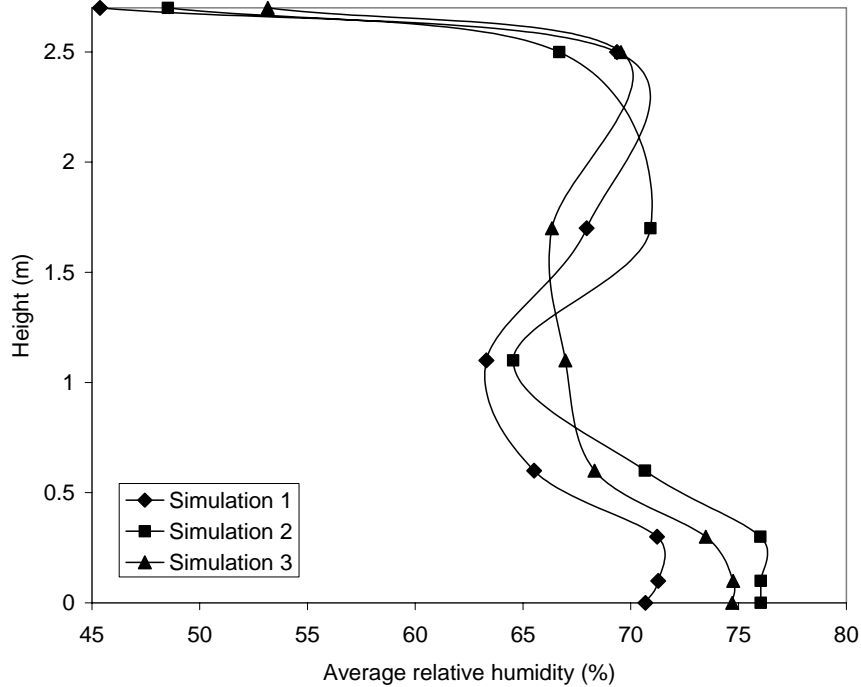
Figure 3.9 Vertical Distribution of Average Relative Humidity for Underfloor System

Figure 3.10 is a comparison among the three underfloor cases in vertical distribution of average contaminant concentration. All three cases show uniform vertical distribution. The lowest level of contaminant concentration was found in inlet-facing-outlet case, resulted from the direct flow from inlet to outlet. The under-desk-inlet case had highest level of contaminant concentration (about 0.00015 kg contaminant/kg air mixture), while the typical case kept it as low as one-third of that level (0.00005 kg contaminant/kg air mixture).

Figure 3.11 shows the velocity fields for typical overhead system (simulation 4). The fresh, cool airflow entered the region through supply inlet on the ceiling with uniform 0.6 m/s speed at 30° downward. Most of the main flow went down induced by natural convection because of its lower temperature.

29
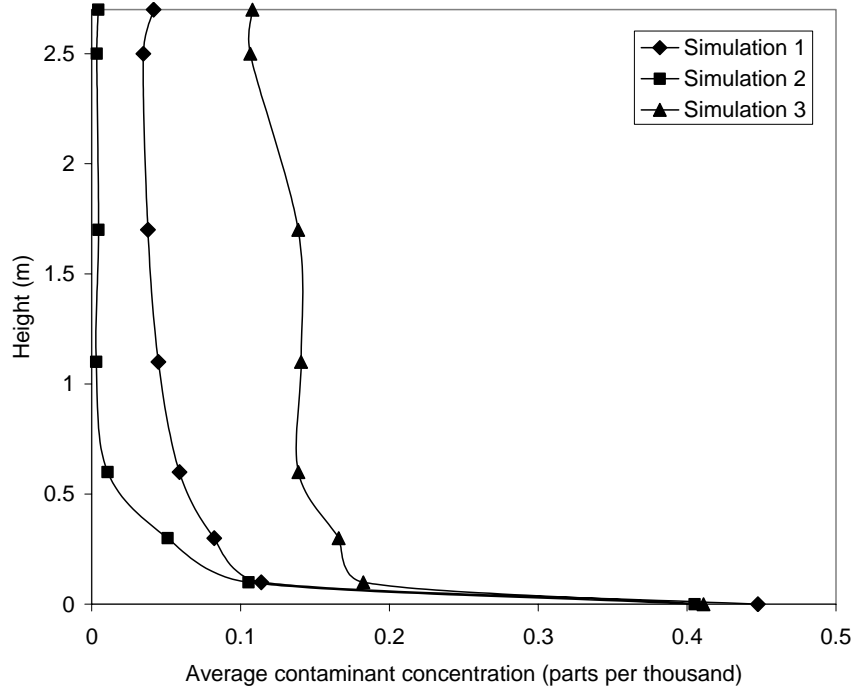
Figure 3.10 Vertical Distribution of Average Contaminant Concentration for
Underfloor System
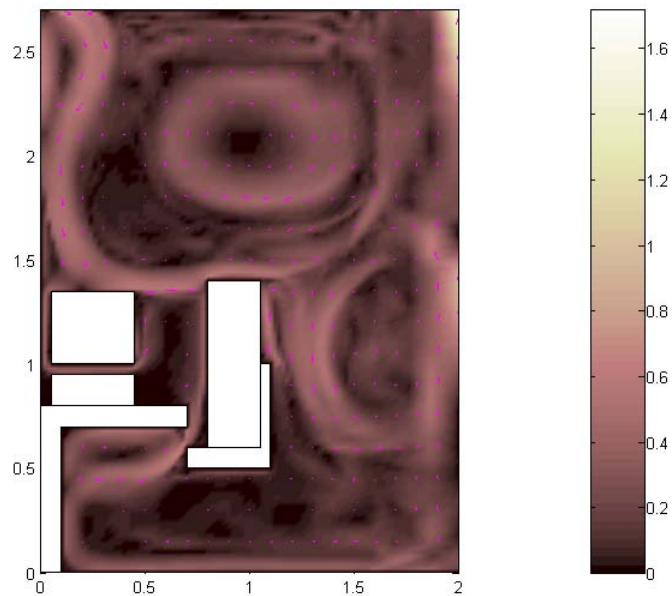
Figure 3.11 Velocity Field for Simulation 4, m/s

30

Under the effects of mixed convection contributed by the main flow itself and by natural convection due to hot surfaces of the person and computer top, an upward flow was formed and went toward the outlet. That effect pushed the main flow bent to the left and they created a circulation in the region above the working space of the person. A small part of the main flow after sweeping the computer top went through the gap between the desk and the person to the floor and rose up a gain on the backside caused a slight slow circulation. Generally, this velocity distribution shows more disturbances than that of the typical underfloor system.

Figure 3.12 gives a view of temperature distribution for typical overhead case. Temperature was distributed more uniformly for this case compare to that of underfloor system, because of the better mixing as a result from the more perturbed velocity field. Lowest temperature region was in the main flow, above and in front of the person's working space. The hot zone next to the computer top was reduced significantly, since the downward main flow sweeping through the zone with cool air removed most of the heat released. However, the higher temperature zone around the person seems to be the same, as heat transport in this zone relied mainly on diffusion rather than convection due to lower air speed, but being compensated by lower inlet temperature. The warmer zone above the person was larger than in typical underfloor case but of lower temperature.

Figure 3.13 shows relative humidity distribution for typical case of overhead air distribution system. For this case, similar to any other case, relative humidity distribution depends strongly on temperature distribution. The relative humidity seems a little higher over all compared to that in the UFAD case, and the zone of low humidity around the person remained the same, as for temperature. Humidity was 65%-75% all over the place.

31
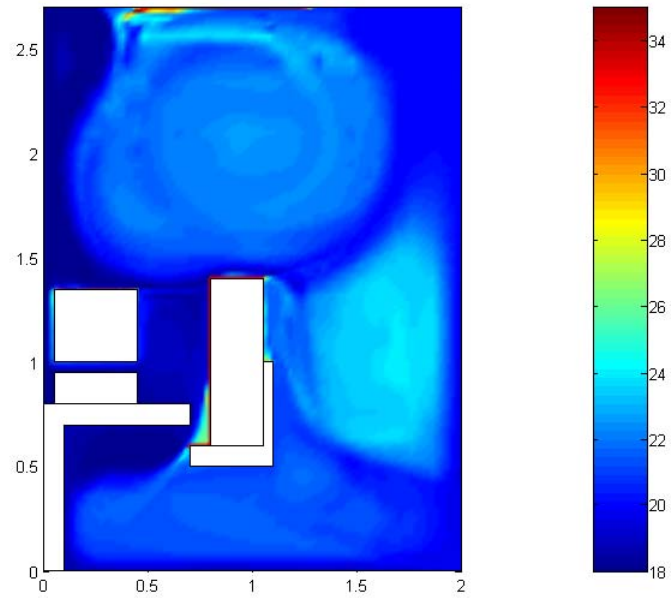
Figure 3.12 Temperature Distribution for Simulation 4, ^{o}C
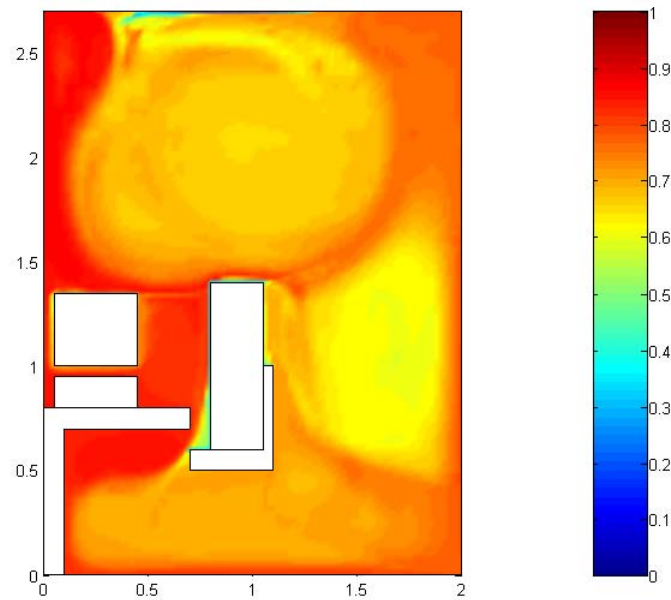
Figure 3.13 Relative Humidity Distribution for Simulation 4

32

Figure 3.14 shows the distribution of contaminant concentration for typical overhead case. The person's working space was almost contaminant free since the force convection flow from the ceiling does not directly induced the contaminant from the floor as well as the strong circulation in the above zone and the through-gap flow drove the slight concentrated contaminant away and kept the high concentration stay close to the floor. The contaminant highly concentrated in a small portion at the right symmetry boundary as the result of a raising flow by natural convection.
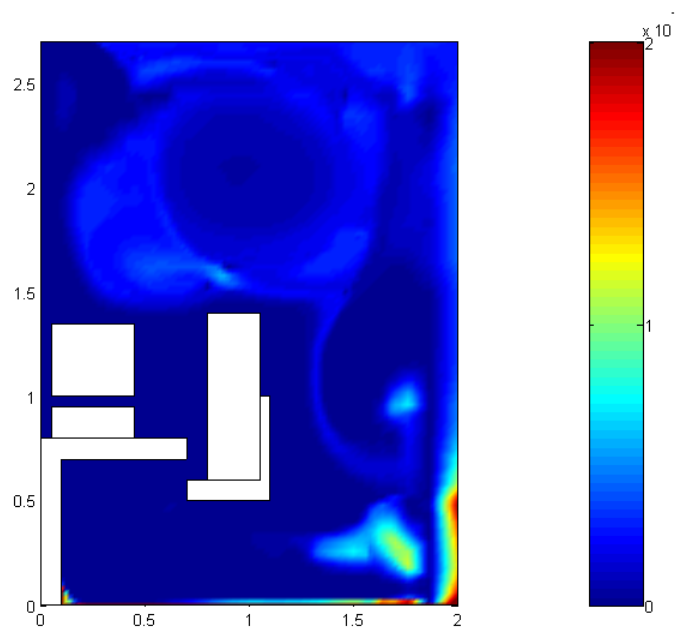
Figure 3.14 Contaminant Concentration Distribution for Simulation 4, kg/kg air

The overhead system alternative cases with different inlet angle affect the airflow response but not too significantly. Figure 3.15 compares the three overhead cases in vertical distribution of air speed. The typical overhead case with inlet angle of 30° shows most moderate distribution with air speed in the range of 0.07m/s-0.25m/s, while the 45°

case (simulation 5) and the 60° case (simulation 6) show large changes in air speed along the height, 0.05m/s-0.25m/s and 0.07m/s-0.27m/s, respectively. The air speeds at the feet were of the same order as we might expect that the change of inlet angle would not affect the lower part of the whole region. The 60° case had lowest air speed at the sitting height.
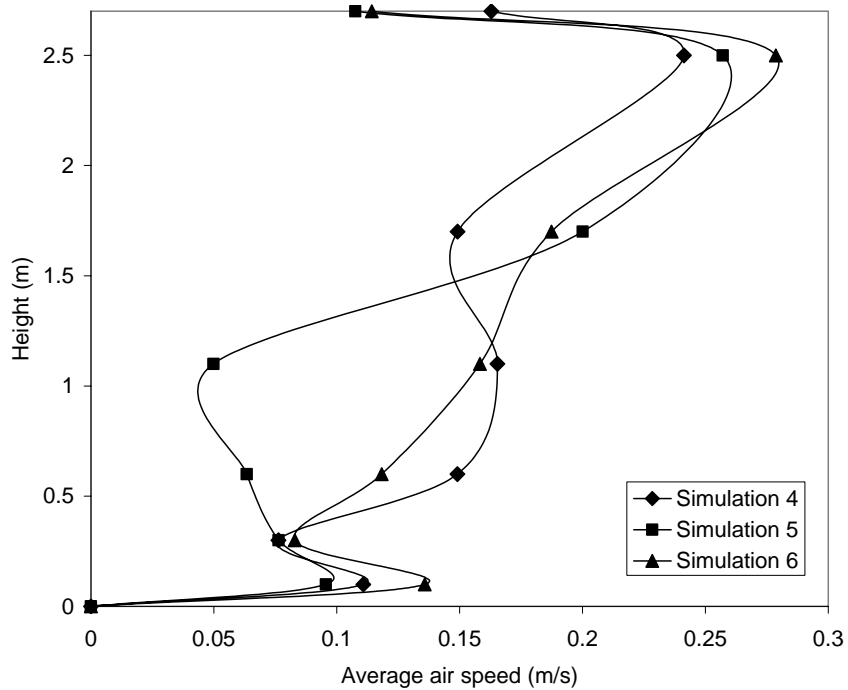
Figure 3.15 Vertical Distribution of Average Air Speed for Overhead System

Figure 3.16 is the plot of vertical average temperature for three overhead cases. It shows that the typical 30° case had higher temperature at the height of sitting person (22^oC-24^oC) while lower at the feet (19^oC-20^oC). The alternative cases had almost the same performance. Their temperature distributions range in 19^oC-23^oC, slightly cold at feet, warmer at the person sitting height and getting colder toward the ceiling, just like the typical overhead case, but cooler over all the total height.

34
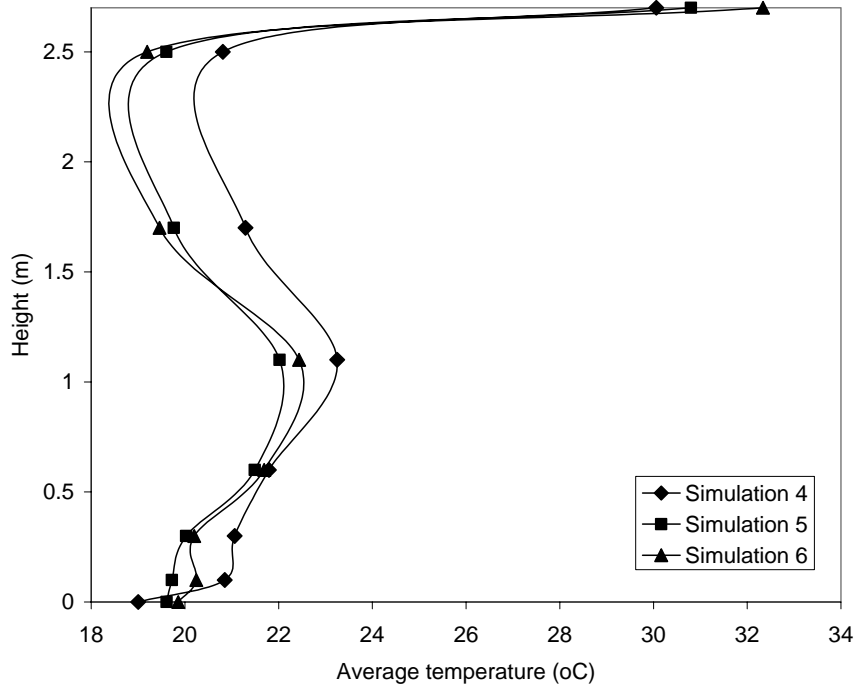
Figure 3.16 Vertical Distribution of Average Temperature for Overhead System

Figure 3.17 presents the vertical distribution of relative humidity for overhead cases. The typical overhead case displays lower relative humidity but more uniform, while the other cases shows higher humid in the higher part of the region. In general, all three curves look very similar in their form. Figure 3.18 shows how contaminant concentrations were distributed vertically for overhead cases. The typical overhead case gave very good characteristics of contaminant control with lowest and almost unchanged concentrated level. The alternative 45° case had higher concentration from the floor up to almost all the working height then reduced toward the ceiling; while in the 60° case, the level increased gradually from the floor, covered the working height and then reduced toward the ceiling.

35
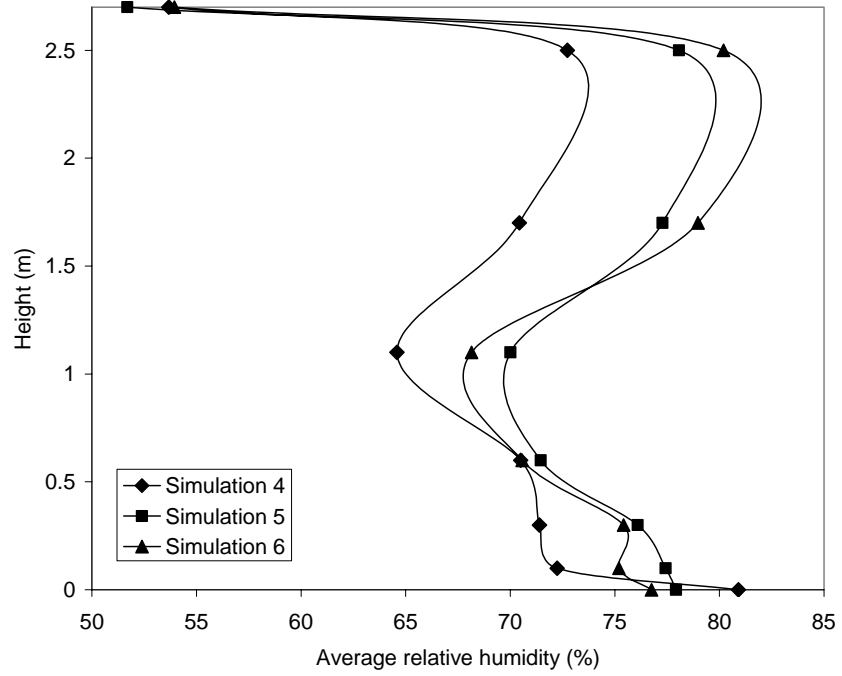
Figure 3.17 Vertical Distribution of Average Relative Humidity for Overhead System
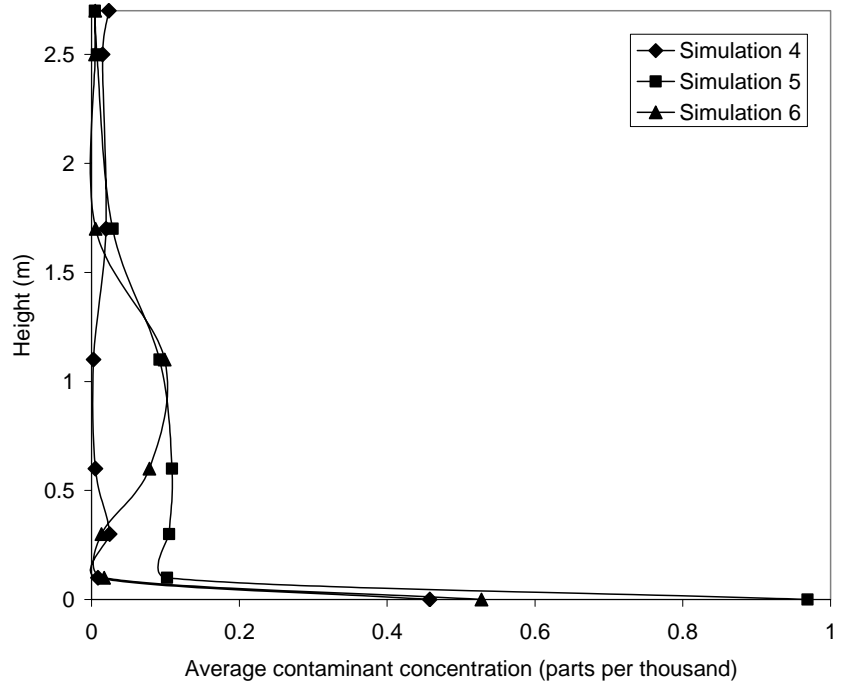
Figure 3.18 Vertical Distribution of Average Contaminant Concentration for

Overhead System

36

Table 3.4 compares summarize results from simulations of the underfloor system to experimental data from [5]. Table 3.5 shows a similar comparison for the overhead system simulation results and those results found in experimental data from [5] for an analogous distribution system. The parameters of interest are the average values of air speed, temperature, relative humidity. The average values were taken for each parameter on all over the computation region.

Table 3.4 Comparison of Average Values of Thermal Comfort to Experimental Data for Underfloor Air Distribution System

Parameter	Simulation No.			Experiment results [5]
	1	2	3	
Air speed (m/s)	0.276	0.360	0.328	0.12
Temperature (^{o}C)	21.7	21.1	21.4	24.4
Relative humidity	66%	69%	68%	60%

Table 3.5 Comparison of Average Values of Thermal Comfort to Experimental Data for Overhead Air Distribution System

Parameter	Simulation No.			Experiment results [5]
	4	5	6	
Air speed (m/s)	0.201	0.173	0.206	0.19
Temperature (^{o}C)	22.3	21.6	21.9	24.9
Relative humidity	70%	72%	72%	65%

37

From the obtained average values, thermal comfort factors as predicted mean vote (PMV) and thermal sensation index were also computed, using the equations Eq. 2.9 – 2.12 and 2.13, respectively.

Figure 3.19 shows the change of PMV and thermal sensation as inlet location changes for the underfloor system model. PMV and thermal sensation values are very close to each other and to the lower limit of the comfort zone. They show a slightly change in thermal comfort level due to inlet location. The higher values of PMV and thermal sensation appear as the inlet is under the seat.
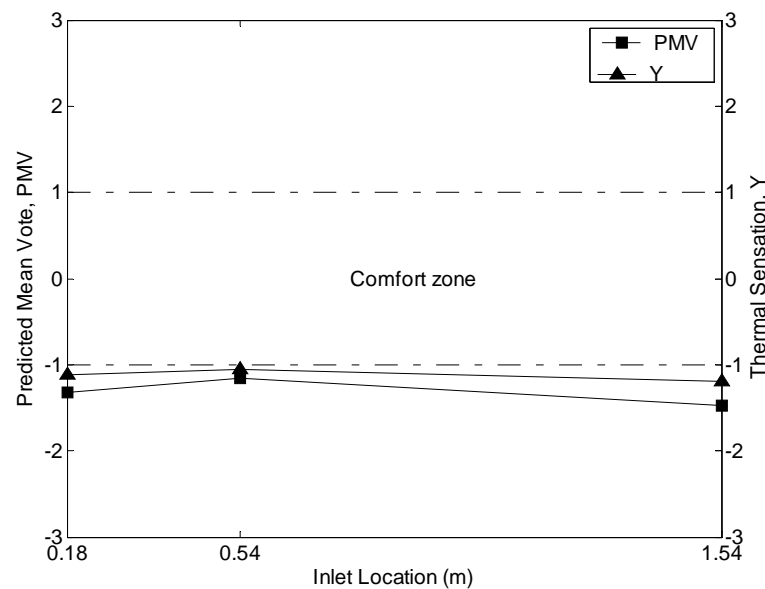
Figure 3.19 Thermal Comfort Factors vs. Inlet Location for Underfloor System

Figure 3.20 shows the change of PMV and thermal sensation as inlet angle changes for the overhead system model. Similar to the underfloor case, PMV and thermal sensations values are very close to each other and slightly change as inlet angle changes. They lay completely inside the comfort zone but still close to its lower limit. The lower

38

thermal comfort level is at the average inlet angle (45°). For both underfloor and overhead system models, there may be extra heat sources on the office floor unaccounted for; including their effects can raise the PMV and thermal sensation for both model and move them inside the comfort zone with a large adjusting margin for designing.
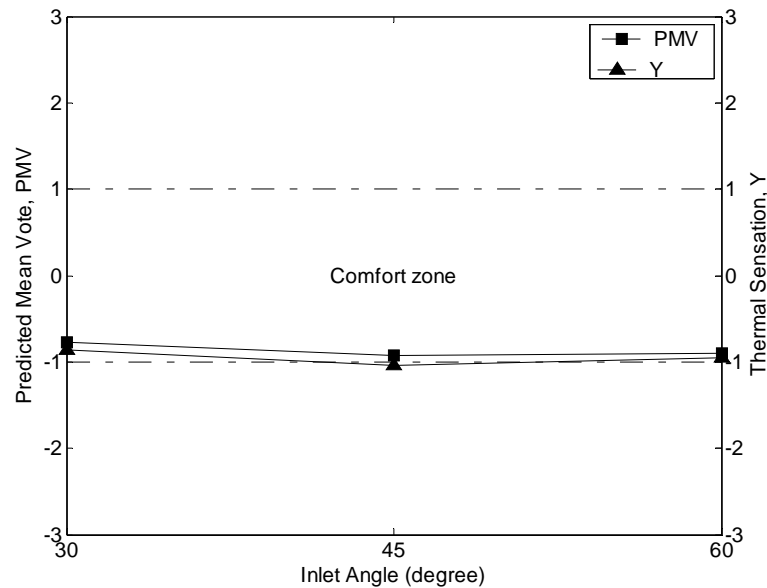
Figure 3.20 Thermal Comfort Factors vs. Inlet Angle for Overhead System

The average air speed for under floor case was higher than that for overhead case, resulted from higher inlet air speed. The average temperatures and relative humidity were almost the same for both cases but slightly lower for underfloor system. PMV and thermal sensation index were inside or close to the comfort zone for both cases. In general, the two systems were satisfied in thermal comfort viewpoint. The simulation results agree with experimental data on most of the relationships between UFAD and overhead system, such as lower average temperature and relative humidity, or higher PMV, for UFAD system compared to overhead system. However, for the same air

39

distribution system, there are differences between simulation and experimental results. For both air distribution systems, experimental data shows that the average temperature was higher than that of simulation results, thus lower relative humidity, and the thermal comfort indices were closer to neutral condition. This could be that the simulations were done for a small cubicle for individual use with symmetric assumed on its boundary to the rest of a large office floor, while the experiments were carried out in a more common zone where there are many more factors interfered. Another reason could be the total heat load was underestimated for not taking into account of many kind heat loads in the common area on an office floor or particular used area, such as sunlight radiation through glass windows, photocopy machines or some other heat generated business equipments.

Table 3.6 shows a comparison of the contaminant removal performance for both systems. On considering average contaminant concentrations, it seems that contaminant concentration can be higher for underfloor system since the inflow at floor-level likely induced the convection of contaminant, also from the floor. The average contaminant concentrations over all as well as at outlet were about of the same order. CRE values were ranging from 0.2 to 0.4 for both systems. For each system, the typical set up shows best control of contaminant removal.

Table 3.6 Comparison of Contaminant Removal Effectiveness

	Underfloor system			Overhead system		
Simulation No.	1	2	3	4	5	6
CRE	0.26	0.33	0.27	0.20	0.21	0.38

40

Figure 3.21 is the plot of vertical distribution of average air speed for the typical cases of the two systems. The distribution profiles for both underfloor and overhead system are similar, as expected the speed value was higher for underfloor system, mostly because of the higher speed at inlet. For both cases, the vertical average speed quickly increased from the floor level, then gradually increased in the zone occupied by the person and the computer, and continued the trend toward the ceiling. It shows that the average air speed was slow down slightly at the person position.
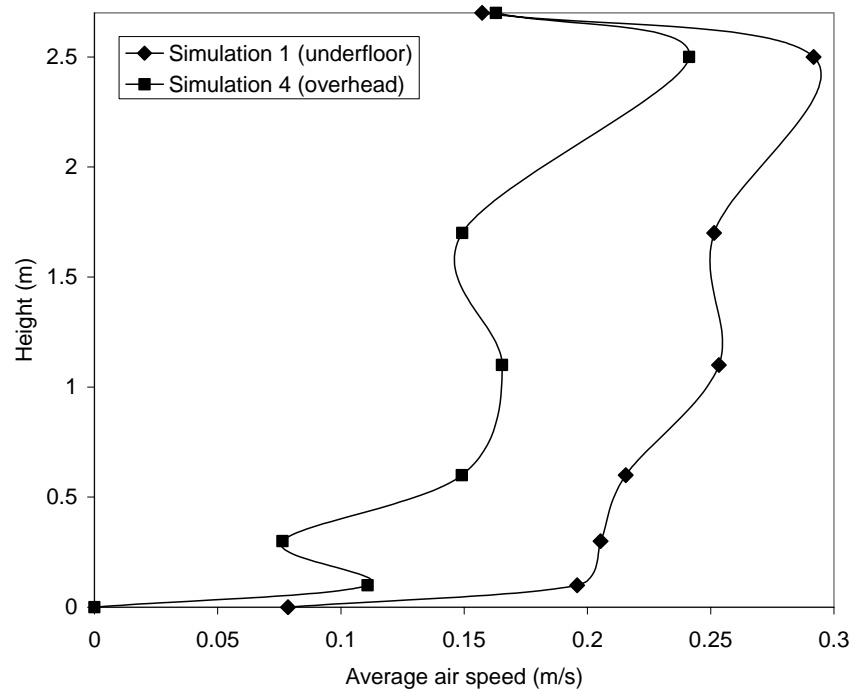
Figure 3.21 Vertical Distribution of Average Air Speed, Underfloor System
vs. Overhead System

Figure 3.22 shows the vertical distribution of average temperature. Both system show the average temperature was higher at the person's position. Most parts of the distribution curves for both systems are identical except the temperature of underfloor

41

system is slightly higher. The difference of vertical average temperature is about 1°C, while the difference of inlet temperature was 2°C.
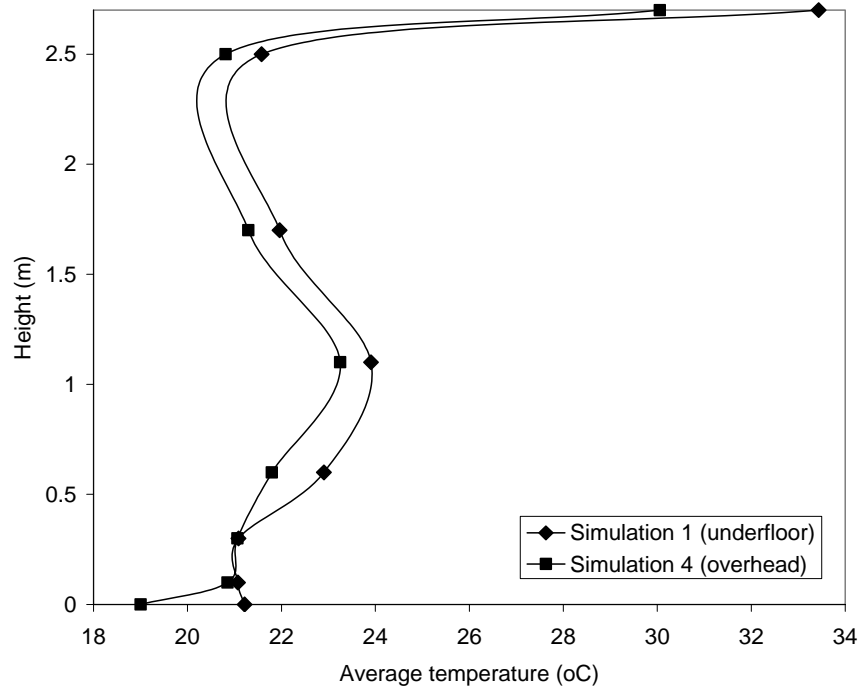
Figure 3.22 Vertical Distribution of Average Temperature, Underfloor System
vs. Overhead System

Figure 3.23 shows the vertical distribution of average relative humidity. Relative humidity was lower at the person's position, and it was lower for underfloor system than for overhead system, i.e. the person feels "dryer" if using underfloor system.

Figure 3.24 shows the vertical distribution of average contaminant concentration. Overhead system has better performance in this aspect. Its distribution profile was at low values but less uniformly distributed along the height, while for underfloor system, almost constant higher concentration distributed along the height.

42
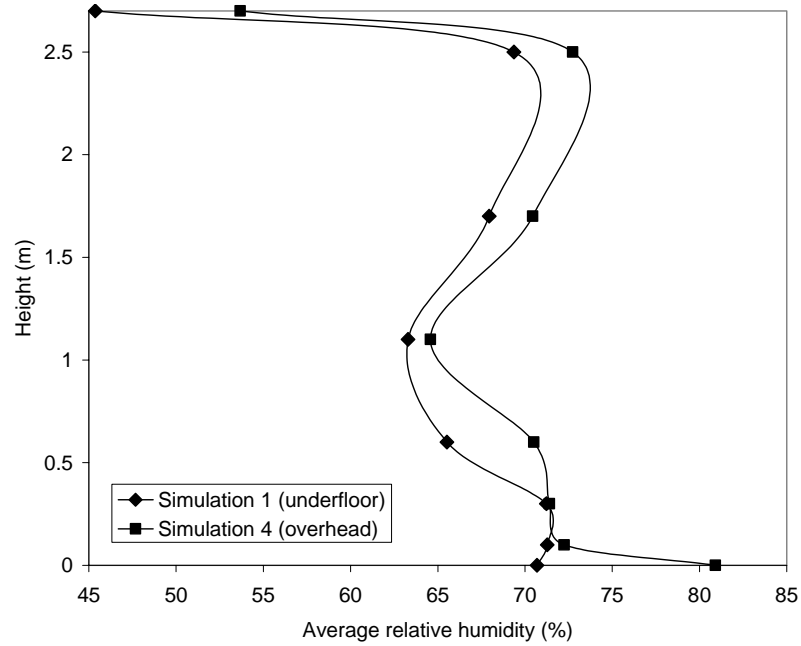
Figure 3.23 Vertical Distribution of Average Relative Humidity, Underfloor System vs. Overhead System
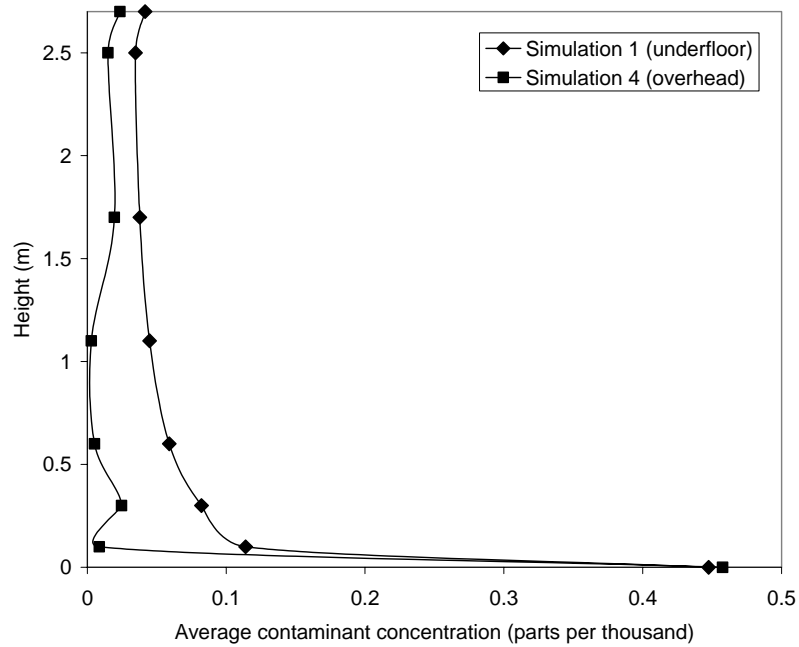
Figure 3.24 Vertical Distribution of Average Contaminant Concentration, Underfloor System vs. Overhead System

43

The performance of each system at the outlet location was studied. These analyses are shown on Fig. 3.25 and 3.26. Figure 3.25 shows the distribution of the vertical component of the velocity vector, which is the normal velocity, along the outlet length. For both systems, the higher vertical velocity was concentrated on the right half of the outlet, i.e. toward the symmetry boundary. Vertical velocity was distributed much more uniformly for underfloor system than overhead system.
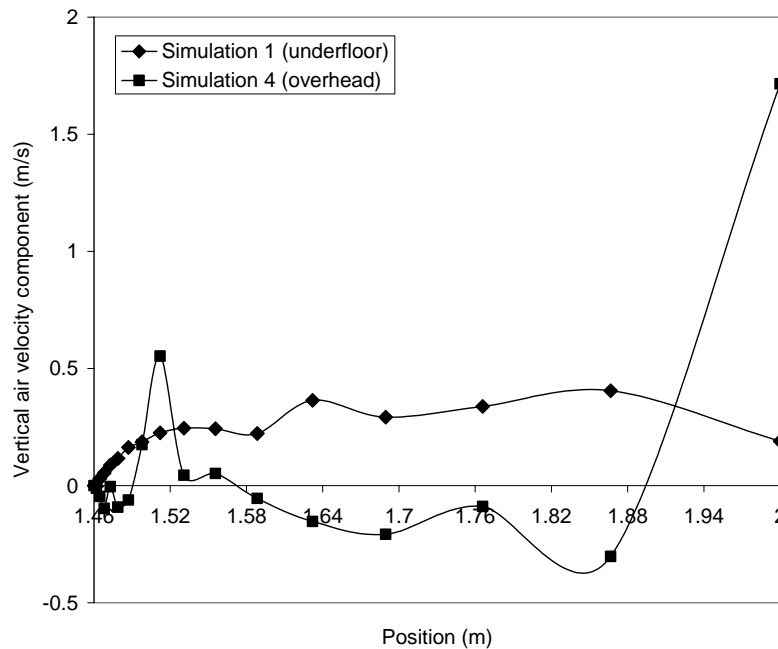
Figure 3.25 Distribution of Vertical Velocity along Outlet Length, Underfloor System vs. Overhead System

Figure 3.26 shows the distribution of contaminant concentration along outlet length. From this figure, we can see that the higher concentration was on the left side of the outlet for underfloor system and on almost uniform over all the outlet length for overhead system.

44
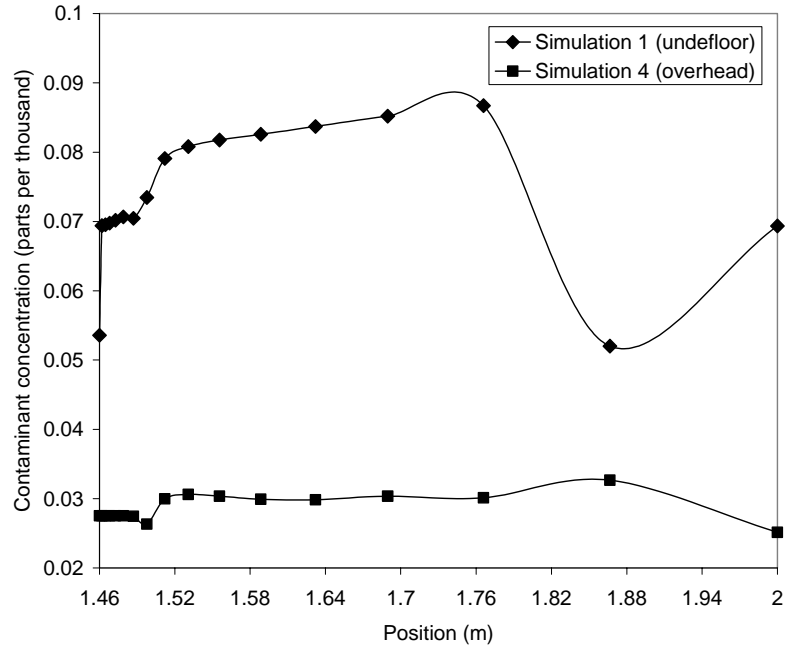
Figure 3.26 Distribution of Contaminant Concentration along Outlet Length, Underfloor System vs. Overhead System

From the above discussion, it is shown that in each system, the typical case is the best setup for that particular system. Both systems satisfy thermal comfort requirements. They have similar performance characteristics in thermal comfort performance. The underfloor velocity field is gentle while the overhead system is more perturbed. The underfloor system has more risk of induced the contaminant at the floor, while the contaminant removal effectiveness of both systems are almost the same.

45

Chapter 4

Predictions of Thermal Comfort and Contaminant Removal in an Operating Room

4.1 Introduction

This part of the work uses airflow simulations to evaluate different ventilation systems on an operating room (OR). This study compares air distribution systems for an operating room by use of computational fluid dynamics (CFD) modeling. The air supply distribution and exhaust arrangements were modeled for a directional air flow system where air moves across the space from the high-pressure supply area to the low pressure exhaust area.

A simplified model of a typical operating room (Fig. 4.1) was considered with inclusion of objects such as surgical lights, operating table, heat sources such as surgical staff (standing) and a patient (lying on operating table), side wall supply grilles and exhaust air grilles. Inlet angle and air return locations were both studied. One and two air-exhaust outlet sites inside the surgical suite were considered. For basic configuration, the model only has the exhaust grills at lower positions on the right wall. The discharge angle for the supply grilles was varied from 0 to 45 degrees. For the two-exhaust outlet configuration, one outlet position was low, close to the floor and the other position was high on the right wall. Simulations with combinations of 30:5, 25:10, 20:15, 15:20, 10:25, and 5:30 flow rates between the two return locations were performed.

46
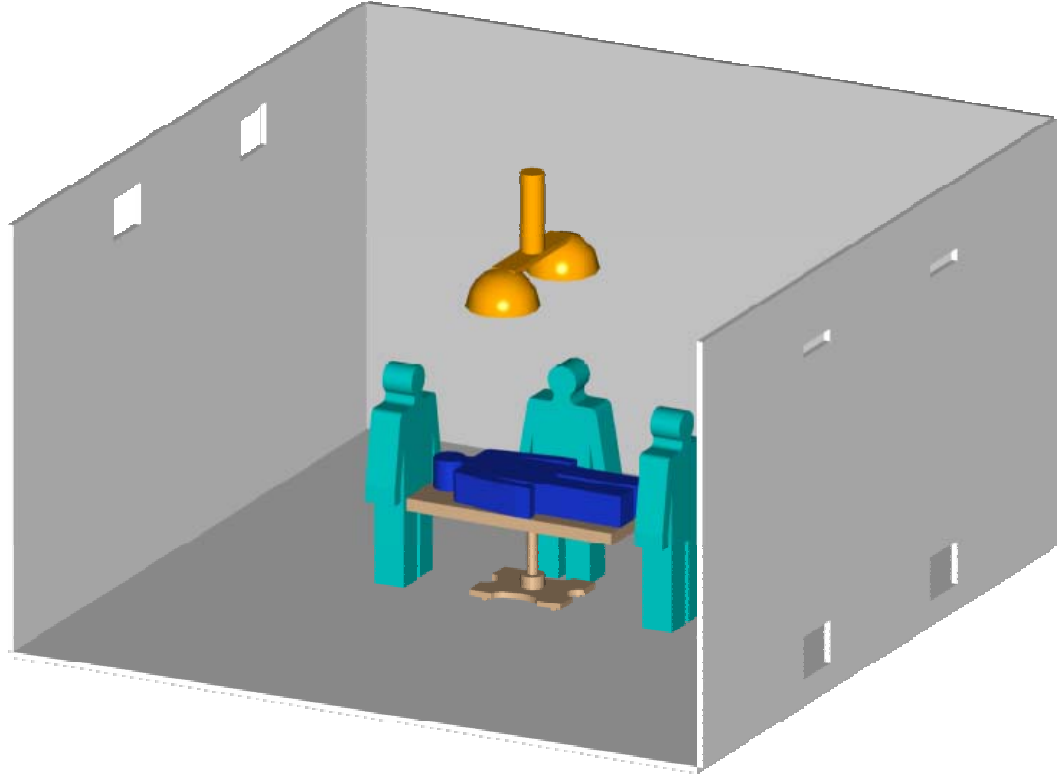
Figure 4.1 Simplified Typical Operating Room

Calculations were done for the operating room's 2D model (Fig. 4.2) in steady-state condition. Predictions for the air movement, room temperature, room relative humidity, and concentration of contaminants within the operating room are shown. Analysis of these predictions is discussed. The supply and exhaust conditions of the ventilation airflow are shown to play an important role in the control of air quality. Results show good agreement with experimental data.

4.2 CFD Model

The operating room was modeled as a 2-D rectangular region with its four boundaries present floor, ceiling and two walls as shown on Fig. 4.2. The essential

47

dimensions are denoted in general forms as L1 to L18 for lengths and A1 for inlet angle. Giving the dimensions in general form makes it flexible for further parameterized investigation, so that alternating essential dimensions can be performed without significant changes in the CFD program.
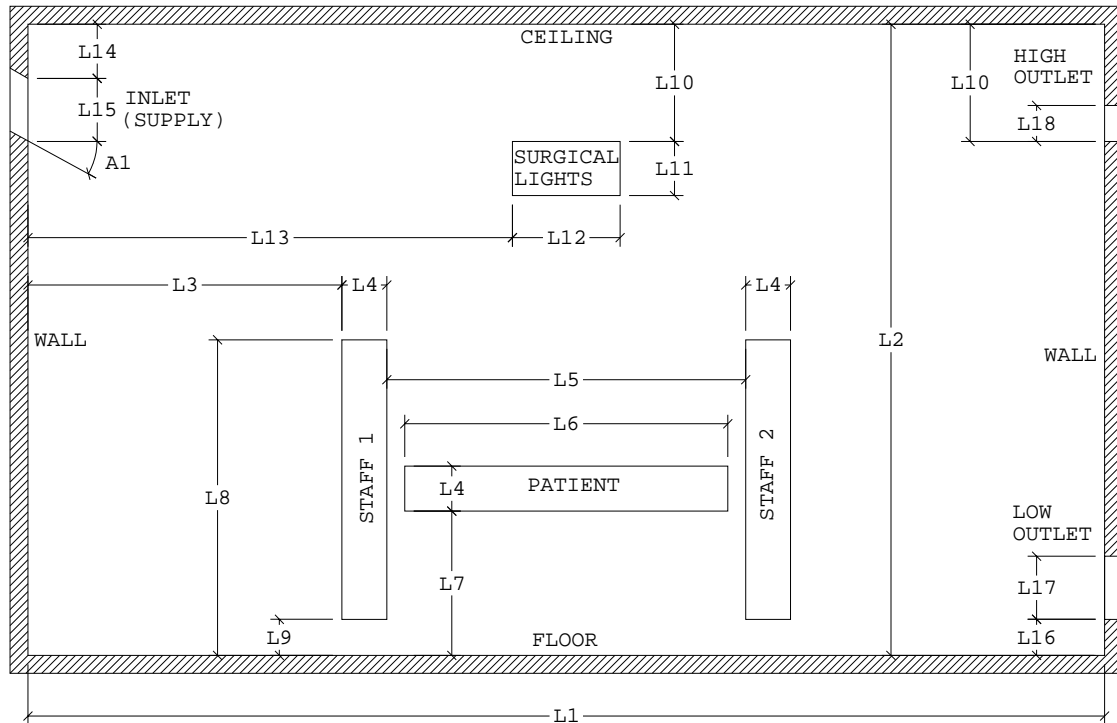
Figure 4.2 Model of Operating Room

The numerical values of the lengths L1 to L16 used for the computations in this paper are given in Table 4.2. The inlet angle A1, and the low and high outlet length, L17 and L18, respectively, are the varying parameters whose effects are to be considered.

The air supply inlet of the room is located at high position on the left wall. For one-exhaust (basic) configuration, there is only one outlet placed at low position on the

48

right wall (low outlet, L17). For two-exhaust outlet configuration, there is also an additional outlet placed at high position on the right wall, at the same height level of and facing the inlet across the room length (high outlet, L18). The sizes of both outlets can be changed but the total size of the two outlets is kept the same as that for the outlet of basic case (and equal to the inlet size, i.e. L15). For the two-exhaust configuration, the high-outlet-to-total-outlet ratio HTR is defined as

$$\text{HTR} = \frac{\text{High outlet area}}{\text{Total outlet area}} = \frac{\text{L18}}{\text{L17} + \text{L18}} = \frac{\text{L18}}{\text{L15}} \tag{4.1}$$

Table 4.1 Dimensions Parameters on Figure 4.1, meter(s)

Name	Length	Name	Length	Name	Length	Name	Length
L1	6.00	L5	2.00	L9	0.20	L13	2.70
L2	3.50	L6	1.80	L10	0.65	L14	0.30
L3	1.75	L7	0.80	L11	0.30	L15	0.35
L4	0.25	L8	1.75	L12	0.60	L16	0.20

To investigate the effect of the supply inlet angle, five cases of inlet angle A1 were considered: 0°, 5°, 15°, 30°, and 45° for the basic configuration (one-exhaust). The inlet angle was measured clockwise from the horizontal direction, i.e. the inlet flow was directed level (0°), down (5°, 15°, 30°, and 45°, toward the floor). For the two-exhaust configuration, six combinations of different sizes of high outlet and low outlet (with unchanged total size) were studied, while the inlet angle was kept at 0°. These simulation cases are summarized in Table 4.2.

49

Table 4.2 Inlet Angle, Outlet Sizes, Outlet Ratios, and Simulation Cases

Simulation number	Inlet angle, A1 (degree)	Low outlet, L17 (m)	High outlet, L18 (m)	HTR (%)
1	0	0.35	0	0
2	5	0.35	0	0
3	15	0.35	0	0
4	30	0.35	0	0
5	45	0.35	0	0
6	0	0.30	0.05	14.3
7	0	0.25	0.10	28.6
8	0	0.20	0.15	42.9
9	0	0.15	0.20	57.1
10	0	0.10	0.25	71.4
11	0	0.30	0.05	85.7

The two walls were kept at constant temperature. The lying patient was modeled as the horizontal rectangle at the middle of the room. Its bottom edge facing the floor modeled the operating table, which is heat and mass insulated. The other three edges modeled the patient's body, which was kept at constant temperature and releasing heat, water vapor, and contaminant as constant fluxes. The standing staffs were modeled by two vertical rectangles at both of the patient's ends. Similar to the patient's model, these two staff models were considered surface at constant temperature and constant water vapor flux. The surgical light was also modeled as a rectangle above the patient, whose

50

bottom edge (facing the patient) was defined as "lamp face" entity, on which the major heat flux went through; and the other three edges were defined as "lamp back" entity, on which a smaller heat flux went through. The boundary conditions on outlet was unknown and to be solved for, as part of the solution of the flow over the whole region. The other boundary conditions left unmentioned were assumed to be zero velocity and totally insulated to heat and mass (e.g. zero velocity and neither heat flux nor mass flux at solid surfaces such as walls, floor, and ceiling; no contaminant flux from the staffs' body, etc.). Details of boundary conditions are given in Table 4.3.

Table 4.3 Boundary Conditions for Operating Room Simulation

No.	Entity	Velocity	Temperature/ Heat flux	Water vapor concentration	Contaminant concentration
1	Inlet	V = 0.4 m/s, (See Table 4.2)	T = 17°C	m_1 = 0.01018 kg/kg air	m_2 = 0 kg/kg air
2	Walls	0	T = 22°C	Flux = 0	Flux = 0
3	Lamp face	0	Flux=100W/m^2	Flux = 0	Flux = 0
4	Lamp back	0	Flux=5 W/m^2	Flux = 0	Flux = 0
5	Patient	0	T = 33°C	Flux = 5E-7 kg/(m^2.s)	Flux = 1E-5 kg/(m^2.s)
6	Staff	0	T = 33°C	Flux = 8E-7 kg/(m^2.s)	Flux = 0
7	Outlet	Unknown	Unknown	Unknown	Unknown
8	Others	0	Flux = 0	Flux = 0	Flux = 0

51

For each simulation, velocity components and temperature were found first by solving the coupled equations Eq. 2.1, 2.4, and 2.5, then the species concentrations (water vapor, contaminant gas) were solved from the equations Eq. 2.2 and 2.3 with known velocity field. The solutions of the finite element analysis generated velocity field, pressure, temperature, water vapor concentration, and contaminant concentration. From pressure, water vapor concentration, and temperature, the relative humidity was computed by using Eq. 2.6 – 2.8. From relevant average parameters, predicted mean vote (PMV) was computed by using Eq. 2.9 – 2.12, thermal sensation by Eq. 2.13, and contaminant removal effectiveness (CRE) by Eq. 2.14.

4.3 Results and Discussion

Figure 4.3 presents velocity distribution for the basic case (simulation 1 in Table 4.2). On Fig. 4.3, velocity field was plotted on the filled speed contour background. It gives the image of how the direction (velocity vector) and magnitude (speed) of the velocity field are distributed. The flow entered the room through the inlet located high on the left wall at 0°, with full speed (0.4 m/s). If there is negligible buoyancy effect, the main stream will flow straight forward at first as shown in [24]. However, for this problem the buoyancy effect is quite strong, which caused the most of the inflow to bend down sharply right at the inlet because of its lower temperature and thus, higher density, compare to the average temperature in the room. The resistances of the stream against this sharp turn created a complicated perturbed region in the higher part of the left end of the room, where the strong separation of streams took place. Most of the inflow went down along the wall and swept along the floor to the outlet. Its top layer mixed with the

52

warmer air next to it, rose at warm surfaces as staffs' bodies under the influence of buoyancy effect, causing upward flows. The warmer upward flows along the staffs' bodies combined with the cooler downward flows along the wall, and supposed to form some slight circulations in the unoccupied space between them. However, these circulations were influenced and deformed by the perturbed region right above it. They combined to make a complicated mixing region. At the inlet, a smaller part of the inflow was pushed up to the ceiling, instead of going down like most part of the inflow. This stream mixed up with the hot air coming up from the surgical site and the lights, swept along the ceiling, and went down at the wall on the right, then exit at the low outlet. Combined with the natural convection flow along the right staff, it created slight circulations in the unoccupied space at the right end of the room.
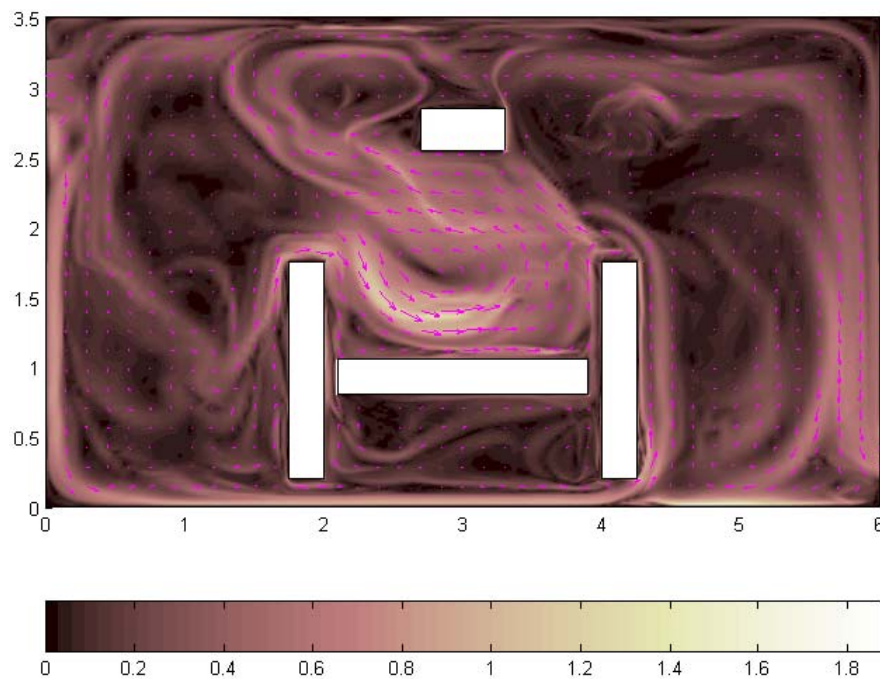
Figure 4.3 Velocity Field for Simulation 1, m/s

53

At the surgical site, stronger circulations were formed, as the results of the a complicated mixing of natural convection along the hot surfaces of people bodies and lights inside the half closed region, interfacing with the cold air around the site from outside of that region. The natural convective flow along the staff on the left went up and got warmer, until it hit the perturbed mixing region above this person, it went down to the lying patient. The buoyancy effect in the gaps between the staffs and the patient was weak because of the resistance of small gaps and the lack of temperature difference, but it could push the flow a little to the right. There, the flow swept along the patient and raised up at the staff on the right, mixed up with the natural convection flow along this person from outside and moved up. This stream was strengthened by the mixed convection flow in the region near the lights and moved to the left. There, it was affected by the perturbed region on its left to form a small region of circulation as an intersection of several streams, then mixed up with the ceiling stream and ran to the right along the ceiling, down the right wall, and exit, as described for the ceiling stream.

Figure 4.4 is the plot of temperature distribution for the basic case. The low temperature of the supply air from inlet is concentrated mostly along walls, ceiling, and floor. There are people, considered as surfaces of constant temperature, and surgical light – as surfaces of constant heat flux. Near these surfaces, temperature changes very steep. In the far surroundings, the temperature distribution seems uniform in general, as this problem is natural convection dominant and this type of convection has better mixing capability than force convection. Another observation is that the temperature distribution mostly looks like the distribution of velocity, i.e. the convective terms are more significant than the diffusive terms in the energy equation.

54
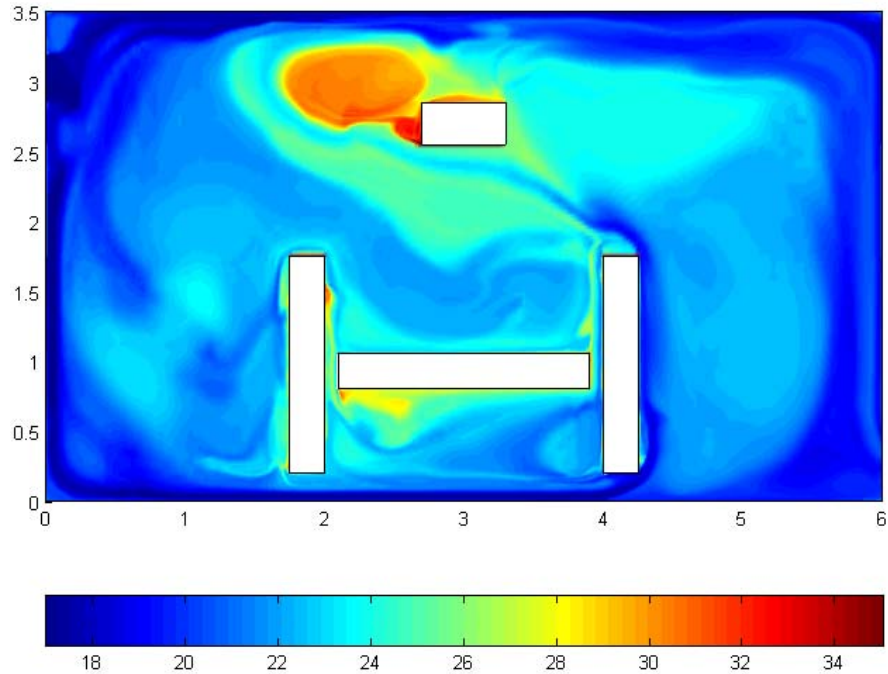
Figure 4.4 Temperature Distribution for Simulation 1, ^{o}C

Figure 4.5 is the plot of relative humidity distribution, a key factor of thermal comfort. Relative humidity is a function of absolute pressure, water vapor concentration, and temperature. Its distribution was computed from pressure, temperature, and water vapor concentration, using ASHRAE procedure as mentioned above. Since the room gage pressure was found very small (at the order of 1 Pa), compared to the atmosphere pressure (as high as 101 kPa), then it does not significantly affect the total (absolute) pressure, and thus almost does not affect the values of relative humidity. Wherever low temperature and high water vapor concentration exist, relative humidity is high also. Near the surgical light, the relative humidity is very low because of the high temperature. There is a high humidity region on the right side of a staff, thus the staff on the right hand side has a more humid surrounding.

55
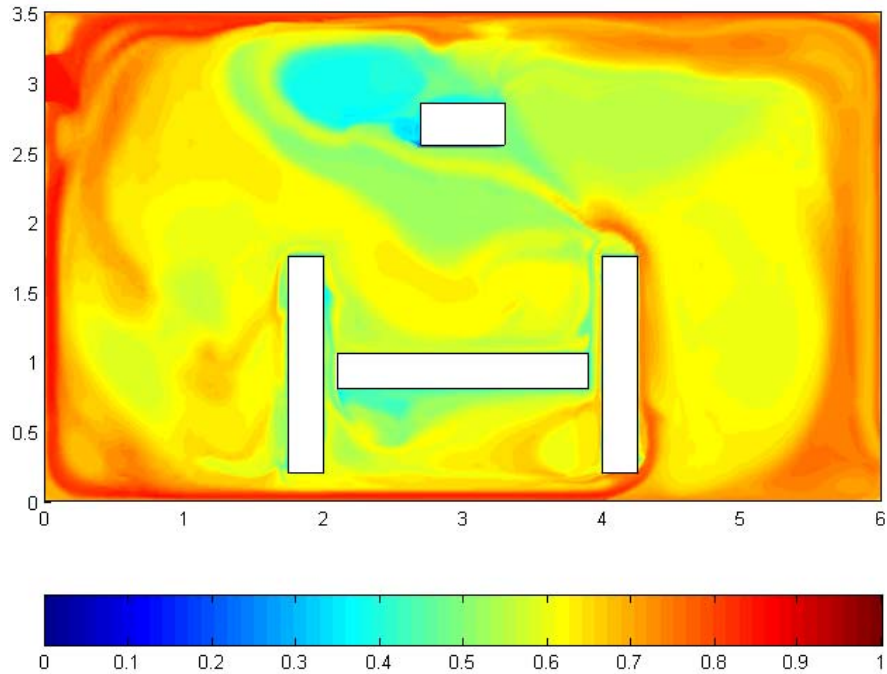
Figure 4.5 Relative Humidity Distribution for Simulation 1

Figure 4.6 shows the plot of contaminant concentration distribution. Contaminant supposedly releases from the body of the patient at a constant rate. It is driven by the concentration gradient, i.e. from patient to the surrounding, especially to the flow of "fresh air". Then the airflow carries contaminant to the outlet. We can see that the process is very effective: the flow swept through the patient from left to right and wash the contaminant away, rose up and carried it to the outlet. Near the patient, the higher concentration is on the right end; therefore, the staff on the right gets a higher contaminant concentration in front of him/her.

Figure 4.7 shows how the contaminant concentration changed for the case of 45°-inlet angle on basic configuration (simulation 5). The average contaminant concentration increased significantly, about 30 times compare to that of simulation 1.

56
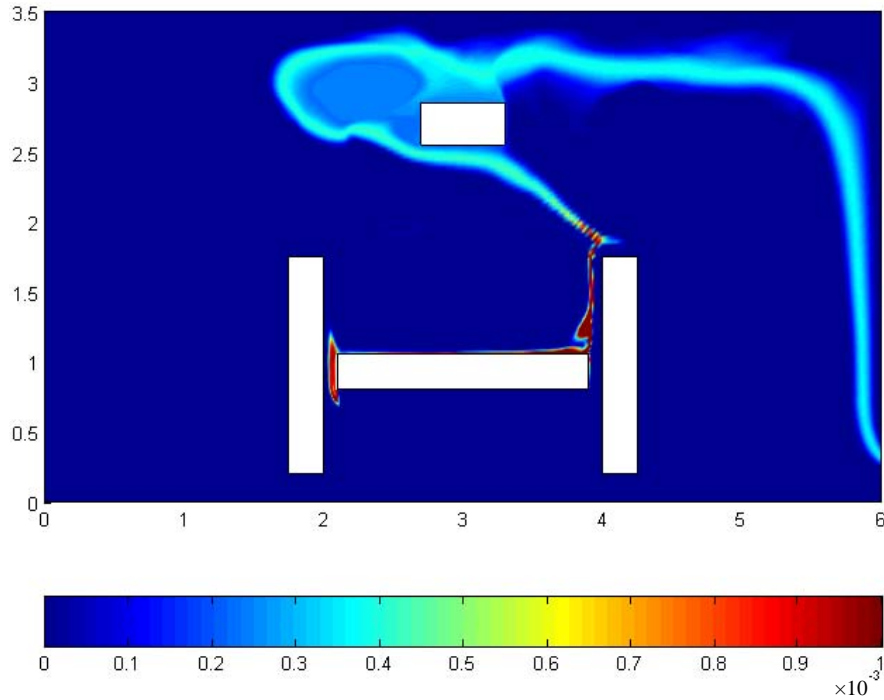
Figure 4.6 Contaminant Concentration Distribution for Simulation 1, kg/kg air

The significant reduction of contaminant concentration in simulation 4 happens because the inlet angle down directed the flow sweeping along the wall, in favor of the downward orientation of the cold air in buoyancy dominant region, whose effect was mostly sweeping the floor rather than going over the surgical site and washed away the contaminant to the outlet. The velocity field is shown on Fig. 4.8 for simulation 5 (basic configuration, 45°-inlet angle).

Figure 4.9 presents the contaminant concentration for the case of two-exhaust configuration with HTR = 71.4% (simulation 10). It can be observed that the contaminant concentration will exit the room by the high outlet if there is one. Although it shows a worse case than the basic case in contaminant removal, it suggests that the use of an additional high outlet may improve the contaminant removal performance of the room.

57
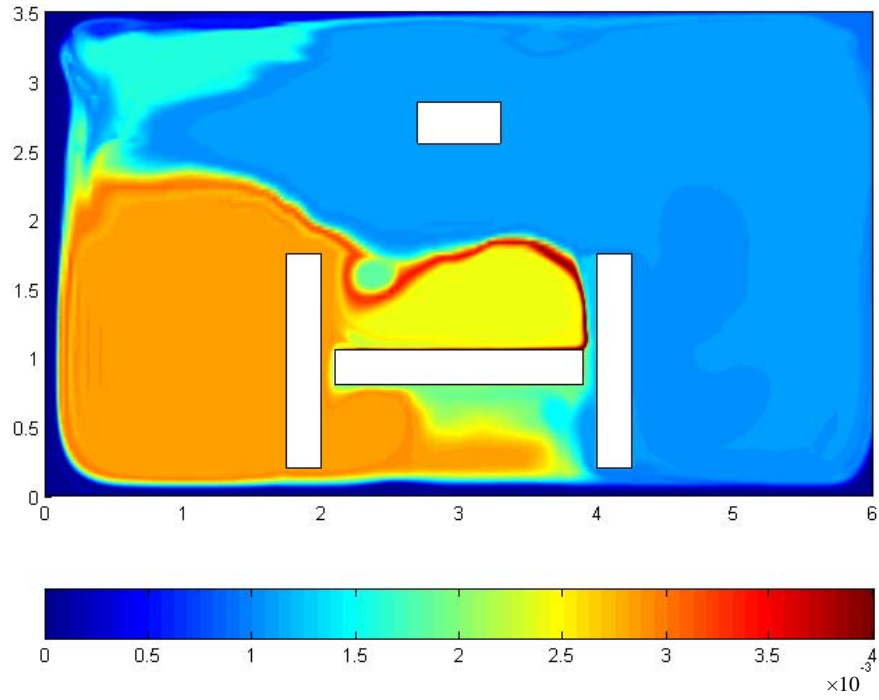
Figure 4.7 Contaminant Concentration Distribution for Simulation 5, kg/kg air
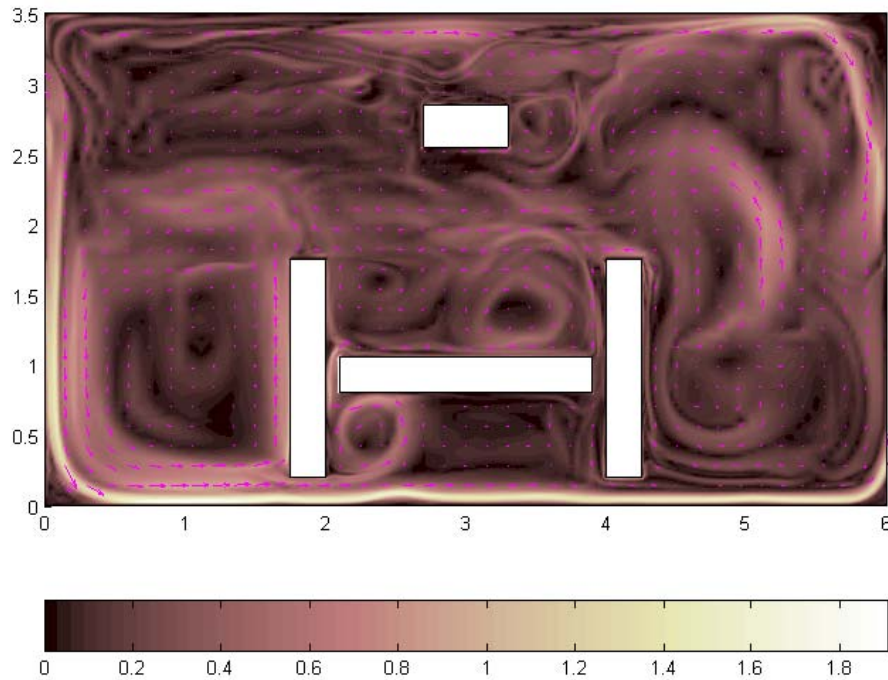
Figure 4.8 Velocity Field for Simulation 5, m/s

58
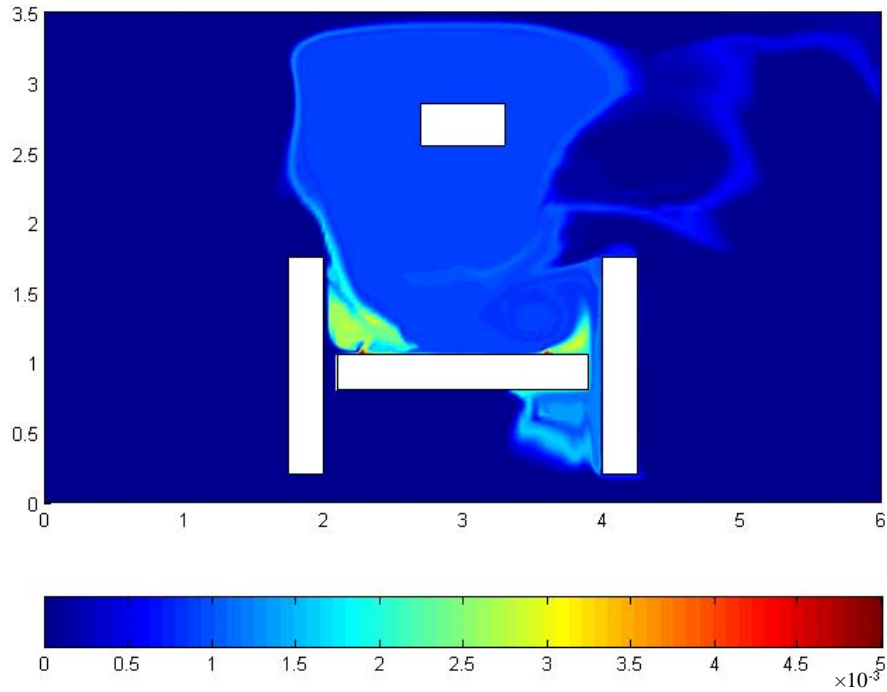
Figure 4.9 Contaminant Concentration Distribution for Simulation 10, kg/kg air

To evaluate the contaminant removal performance of the room, the average contaminant concentration and the contaminant removal effectiveness (CRE) were considered. The average value for each simulation was taken for all over the computation region.

Figure 4.10 shows that the average contaminant concentration increases as inlet angle increases. Thus for this kind of buoyancy dominant airflow in operating room, increasing the inlet angle may induce higher contaminant concentration. If the buoyancy effect is negligible (force convection dominant), the increase of inlet angle (directed down) may help reduce the contaminant concentration [24], because it directs the main flow to wash through the surgical site. However, if buoyancy effect cannot be neglected, which is now considered in the simulations, the basic case of 0°-inlet angle itself is

59

equivalent to a case of several tens of degree down in problem with only force convection, since the buoyancy effect tends to pull the inflow stream down already.
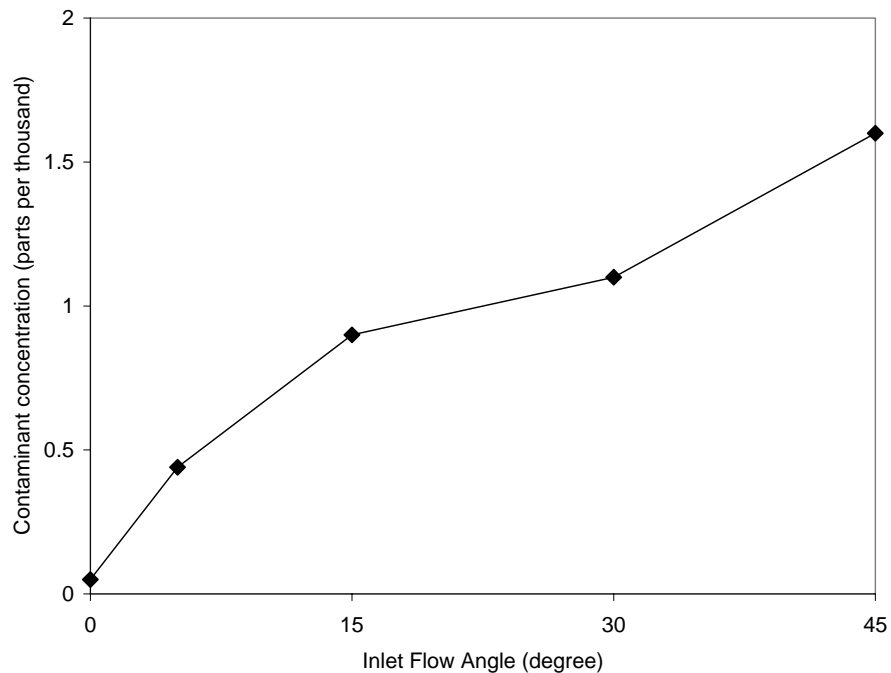
Figure 4.10 Average Contaminant Concentration vs. Inlet Angle for Basic Configuration

On Fig. 4.11, CRE decreases significantly from the basic case (0°-inlet angle) to higher inlet angle then increases a little after 30°. Increasing the inlet angle (down) always causes negative effects on contaminant level control.

Figure 4.12 shows how contaminant concentration changes as a function of outlet ratio HTR. It does not show a clear relationship between the two, with the average contaminant concentration going up and down as HTR increases, and all values were higher than the basic case with one low outlet only. How ever, the contaminant removal effectiveness is affected by the outlet ratio as shown on Fig. 4.13.

60
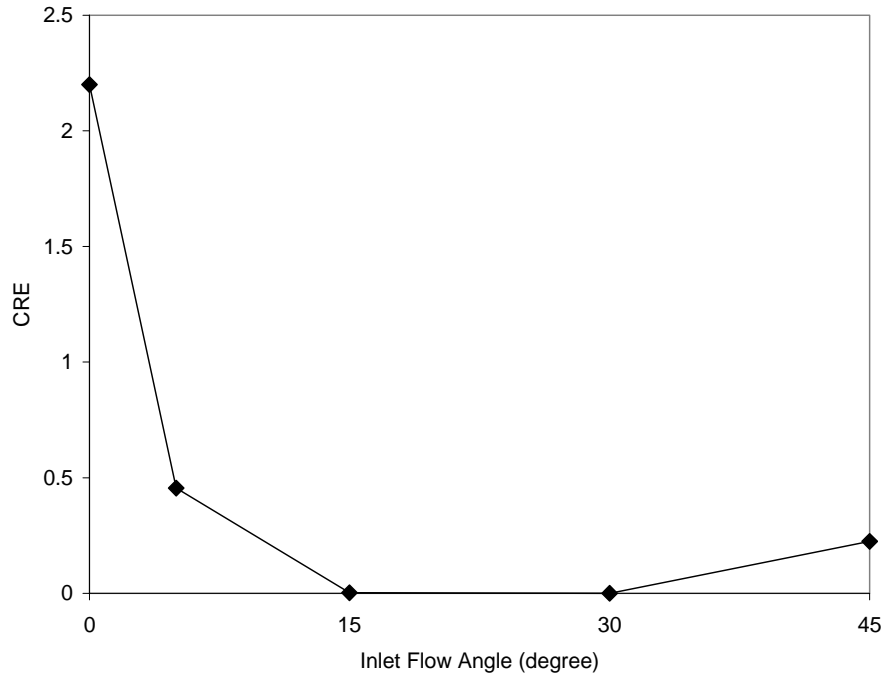
Figure 4.11 Contaminant Removal Effectiveness vs. Inlet Angle for Basic Configuration
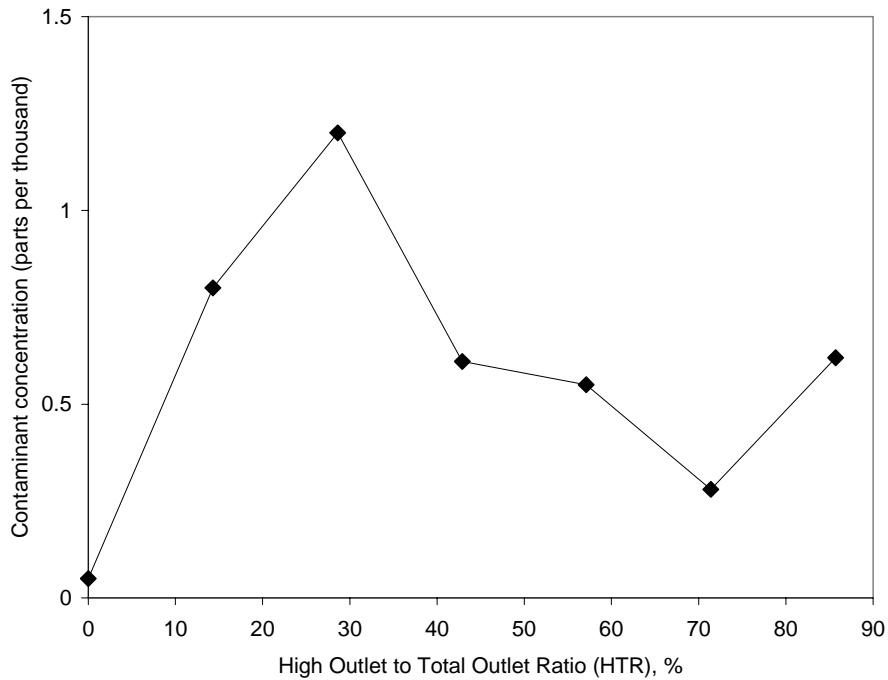
Figure 4.12 Average Contaminant Concentration vs. Outlet Ratio for Two-Exhaust

Configuration

61

Figure 4.13 shows that as HTR increases, the contaminant removal effectiveness (CRE) increases, after a slight drop-down at first from the basic case (HTR = 0%). This response can be used for controlling the contaminant concentration level, but with caution to reduce the negative effect of increasing contaminant level.
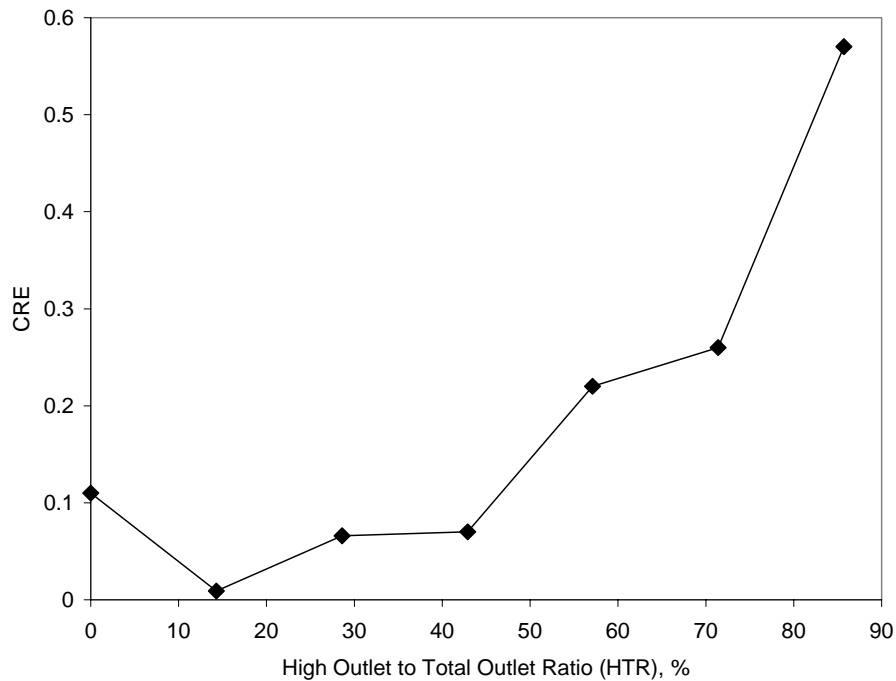
Figure 4.13 Contaminant Removal Effectiveness vs. Outlet Ratio for Two-Exhaust Configuration

Table 4.4 shows a comparison of average essential thermal comfort parameters (air speed, temperature, and relative humidity) for different inlet angles. As inlet angle increases, average air speed ranges in 0.2 m/s – 0.4 m/s, average temperature, 20°C – 23°C, and relative humidity, 61% – 69%. Table 4.5 shows a comparison of air speed, temperature, and relative humidity for different high outlet to total outlet ratio (HTR).

62

Table 4.4 Average Air Speed, Temperature, Relative Humidity vs. Inlet Angle for
Basic Configuration

Inlet angle, A1	0°	5°	15°	30°	45°
Air speed (m/s)	0.25	0.43	0.35	0.36	0.27
Temperature (^{o}C)	22.1	20.6	22.9	20.9	23.0
Relative humidity (%)	61.2	67.7	66.0	68.5	61.6

Table 4.5 Average Air Speed, Temperature, Relative Humidity vs. Outlet Ratio for
Two-Exhaust Configuration

Outlet Ratio, HTR	14.3%	28.6%	42.9%	57.1%	71.4%	85.7%
Air speed (m/s)	0.41	0.46	0.59	0.35	0.35	0.33
Temperature (^{o}C)	23.7	22.5	21.9	23.1	20.6	23.6
Relative humidity (%)	60.1	60.9	62.3	69.2	68.7	67.0

As HTR increases and 0°-inlet angle, average air speed ranges in 0.3 m/s – 0.6 m/s, average temperature, 20°C – 24°C, and relative humidity, 60% – 69%.These parameters are in the reasonable range for an operating room in hospital [18, 21]. It can be expected that the change of inlet angle and HTR does not affect the thermal comfort of the room very significantly, and HTR has stronger affect than that of inlet angle.

For assessing the thermal comfort level of the room, we consider its thermal sensation index and predicted mean vote (PMV). Figures from 4.13 to 4.16 show the thermal sensation and PMV as functions of inlet angle and outlet ratio. Both of them are parameters for assessing thermal comfort, but at slightly different viewpoints. Thermal

63

sensation expresses the correlation between comfort level, temperature, humidity, sex, and length of exposure, while predicted mean vote (PMV) provides a measure of how people are likely to respond to different environments based on the conditions of a particular individual including metabolic rate, clothing, and air velocity besides temperature and humidity. Thermal sensation and PMV use the ASHRAE scale, which is an index from -3 (very cold) through 0 (neutral) to +3 (very hot). The comfort zone can be taken from -1 (slightly cool) to +1 (slightly warm), which is shown on Figures 4.9 through 4.12 as two level dash-dotted lines.

Figure 4.14 shows how the thermal sensation changes as inlet angle changes. There is a decrease at first and then the thermal sensation slightly increases. It suggests that the thermal sensation does not depend much on inlet angle. The thermal sensation curve was in the limit of the comfort zone, left a wide margin for design, which may raise the curve deeper inside the comfort zone.

Figure 4.15 shows the predicted mean vote (PMV) for patient and staff as inlet angle changes. It decreases at first as inlet angle increases up to about 5° then increases as inlet angle increases, ranging from cold to slightly cool for patient and slightly cool to slightly warm for staff. The thermal sensation index from Fig. 4.13, as a factor for assessing the environment generally can be observed to be laying between PMV curves for patient and staff. At any inlet angle, staff was always in comfort zone while patient is not comfortable (cold).

Figures 4.16 and 4.17 present the thermal sensation and PMV as functions of outlet ratio HTR. Although they are not very sensitive to outlet ratio, it can be found that their slight variations are quite interesting.

64
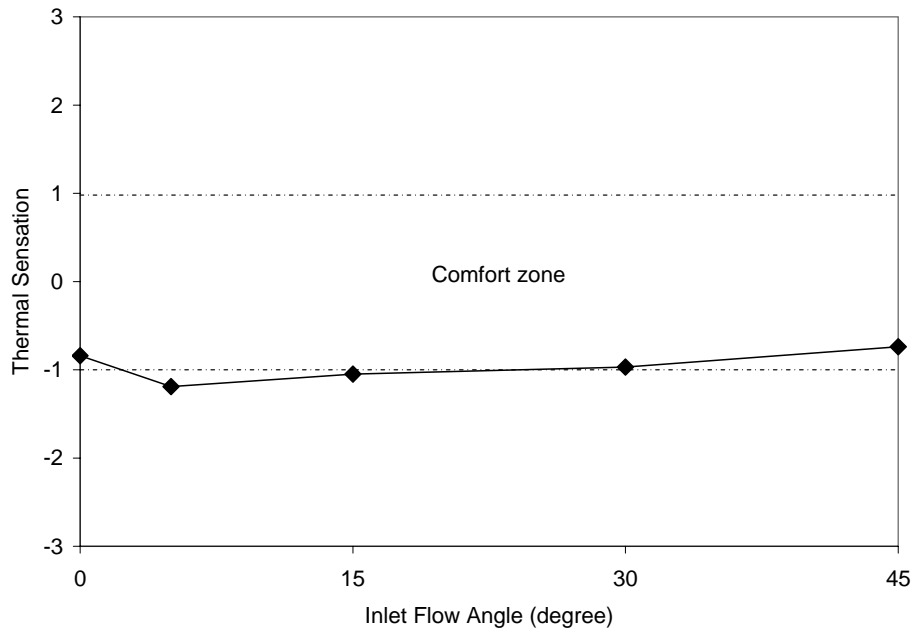
Figure 4.14 Thermal Sensation Index vs. Inlet Angle for Basic Configuration
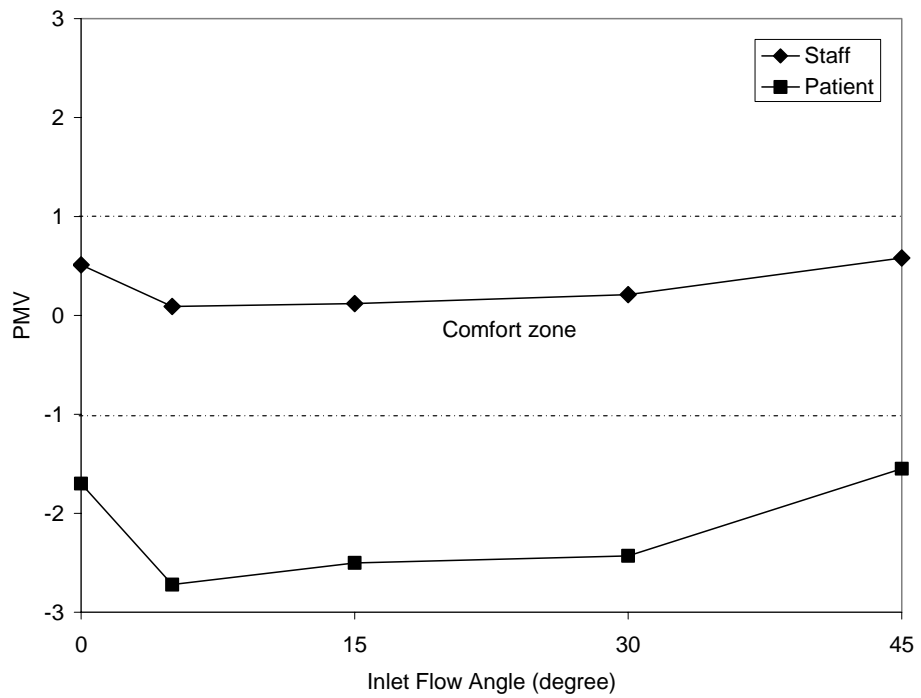
Figure 4.15 Predicted Mean Vote vs. Inlet Angle for Basic Configuration

65

www.manaraa.com
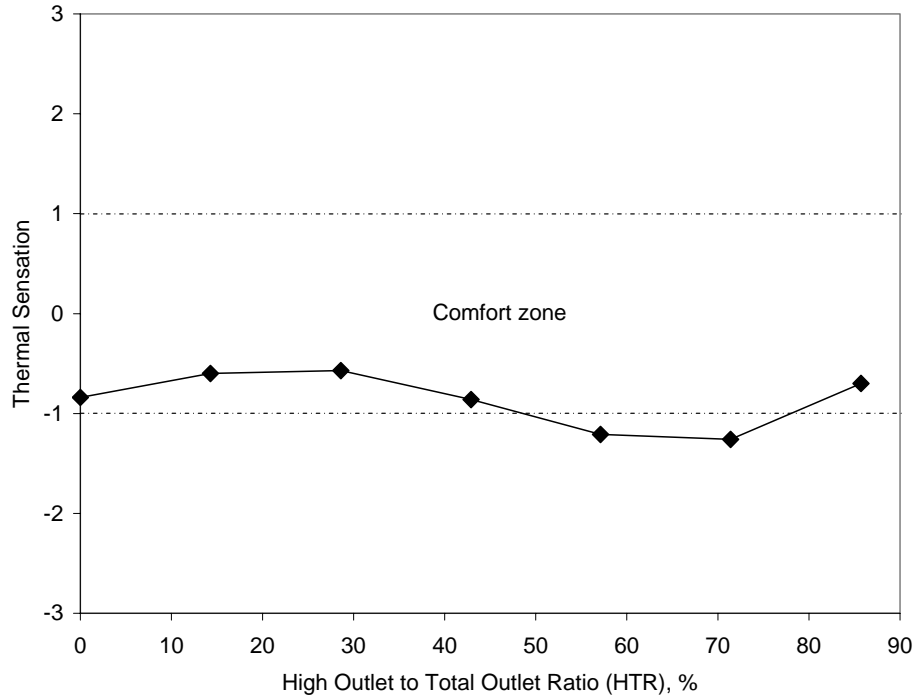
Figure 4.16 Thermal Sensation Index vs. Outlet Ratio for Two-Exhaust Configuration
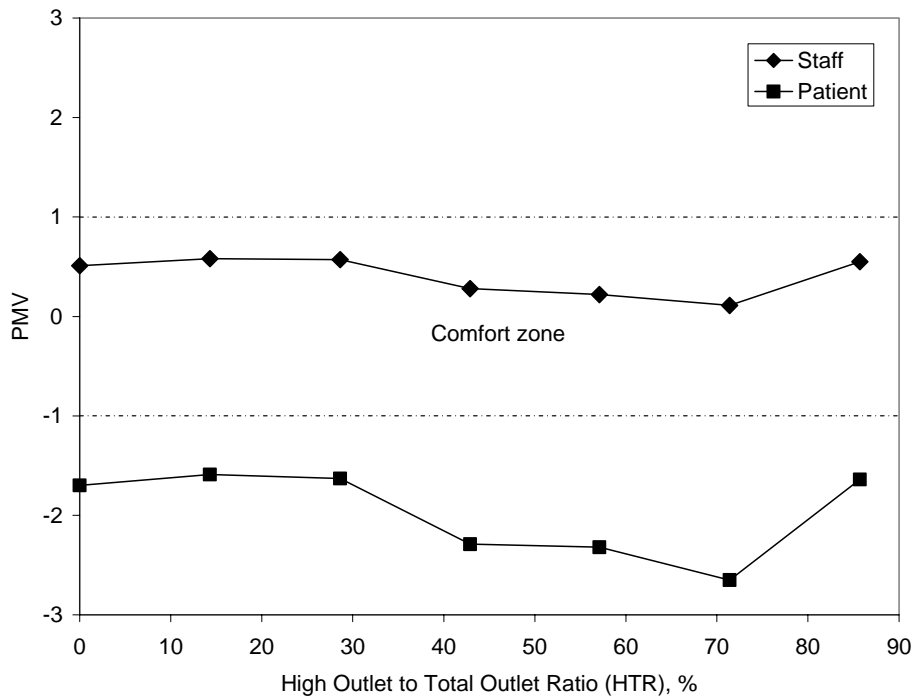
Figure 4.17 Predicted Mean Vote vs. Outlet Ratio for Two-Exhaust Configuration

66

As HTR increases, thermal sensation increases at first then decreases, then increases again. The same response was also observed on PMV curves of patient and staff. Similar to the case of varying inlet angle, staff was always in comfort zone while patient is not comfort (cold).

The average temperature and relative humidity were compared with those from experimental data given in [18, 21] in Table 4.6.

Table 4.6 Comparison of Average Temperature and Relative Humidity to
Experimental Data

Simulation results											
Simulation number	1	2	3	4	5	6	7	8	9	10	11
Temperature (^{o}C)	22	21	23	21	23	24	23	22	23	21	24
Relative humidity (%)	61	68	66	69	62	60	61	62	69	69	67
Experimental data from [21], based on 2 operating rooms											
Temperature (^{o}C)	Ranges from 19.5 to 25										
Relative humidity (%)	Ranges from 24% to 63.5%										
Experimental data from [18], based on 20 operating rooms											
Temperature (^{o}C)	Ranges from 18.6 to 24.5										
Relative humidity (%)	Ranges from 27% to 53%										

The data from [21] and [18] are collected from 2 and 20 operating rooms, respectively. The average temperature from the numerical simulation shows reasonably good agreement with experimental data. The average relative humidity from CFD

67

solution is higher than that of experimental data. The relative humidity is very sensitive to the changes of temperature and water vapor concentration. The averaging for CFD solution included all regions inside the room, while the experimental data were collected at some specifics locations near the working spaces, where the temperature was higher thus relative humidity was lower. Besides, there are some points in experimental data where relative humidity values were higher than the CFD average value.

Chapter 5

Conclusions and Recommendations

5.1 Simulation of the Office Room

Two air distribution systems widely used for office rooms with typical and alternative cases were considered, showing the responses of airflow with different system and setup. Both simulated cases showed comparable thermal sensation. PMV was close to comfort zone in both cases. The comparison of results from two simulations shows that the UFAD system has some advantages to overhead system, especially in contaminant removal. Improvement in indoor air quality was expected by delivering the fresh supply air near the occupant at floor level, allowing an overall floor-to-ceiling airflow pattern to more efficiently remove contaminants from the occupied zone of the cubicle. Comparison to experimental data shows good agreement among systems of similar airflow characteristics. The simulation results suggest that CFD modeling can be satisfactory used for predicting airflows in an office.

5.2 Simulation of the Operating Room

The CFD simulations gave a good understanding of multi-component flow in an operating room. From the above discussion, it was found that the change of inlet angle down could have negative effects on the contaminant removal characteristics of the OR.

69

The basic case of 0° inlet angle might be the best choice. Two-exhaust configurations can be employed for improving CRE with careful considerations since it may increase the total level of contaminant concentration. A bad choice of higher outlet size may cause more trouble than benefit. The lower outlet should still be the main outlet while the higher one can be considered as a regulating mechanism. A ratio of higher outlet-to-lower outlet area at about 0.7 would improve the contaminant removal characteristics without raising the contaminant level too high. Inlet angle and outlet ratio are two main factors to control the contaminant level and need to be selected concurrently. Thermal comfort factors, however, are not greatly affected by inlet angle and outlet ratio. In OR's, it seems that the patient always feel colder than the staff. Since thermal comfort for patient and staff vary in a narrow range, the inlet temperature can be raised a few degrees to make the thermal sensation and PMV go into the comfort zone for both, with the patient at the lower limit and the staff at the higher limit of the comfort zone.

5.3 Recommendations

For improving the CFD modeling to simulate better the real phenomena of airflow and heat transfer in real life air conditioned rooms, the following approach can be considered:

- Three-dimensional modeling: 3-D model will show better the space interaction of the fluid flow and heat transfer phenomenon.
- Taking into account the equipments in the rooms as obstacles to the fluid flow as well as heat transfer surfaces where needed. This will give distribution of the parameters of interest closer to the real environment.

70

References

[1] Woods J.E., 2004, "What real-world experience says about UFAD alternatives," ASHRAE Journal, *46* (2), pp. 3-15.

[2] Webster T.W., Bauman F., and Reese J., 2002, "Underfloor air distribution: thermal stratification," ASHRAE Journal, *44* (5), pp. 28-33.

[3] Stanke D., 2001, "Turning air distribution upside down… underfloor air distribution," Engineers Newsletter, *30* (4), http://www.trane.com/.

[4] Halza J.M., 2003, "Underfloor & overhead ductless VAV systems," ASHRAE Journal, *45* (11), pp. 43-48.

[5] Fukao H., Oguro M., Ichihara M., and Tanabe S., 2002, "Comparison of underfloor vs. overhead air distribution systems in an office building," ASHRAE Transactions, *104* (1), pp. 64-76.

[6] Webster T., Bannon R., and Lehrer D., 2002, "Teledesic broadband center field study," Center for the Built Environment (CBE), Summary Report April 2002.

[7] Chow W.F., and Fung W.F., 1996, "Numerical studies on indoor air flow in the occupied zone of ventilated and air-conditioned space," Building and Environment, *31*, pp. 319-344.

[8] Bauman F.S., 1999, "Giving occupants what they want: guidelines for implementing personal environmental control in your building," Proceedings at World Workplace 99, Los Angeles, CA.

[9] Emmerich S.J., 1997, "Use of computational fluid dynamics to analyze indoor air quality issues," NISTIR 5997, Building and Fire Research Laboratory, National Institute of Standards and Technology, Gaithersburg, MD.

[10] Gadgil A.J., Finlayson E.U., Hong K.H., and Sextro R.G., 1999, "Commercial CFD software capabilities for modeling a pulse release of pollutant in a large indoor space," Proceedings of Indoor Air '99, Edinburgh, *4*, pp. 749.

[11] Hirnikel D.J., Lipowicz P.J., and Lau R.W., 2002, "Predicting contaminant removal effectiveness of three air distribution systems by CFD modeling," ASHRAE Transactions, *108* (1), pp. 350-359.

71

[12] Fanger P.O., 1970, *Thermal Comfort analysis and applications in environmental engineering*, McGraw-Hill, New York.

[13] Rohles F.H. Jr. and Nevins R.G., 1971, "The nature of thermal comfort for sedentary man," ASHRAE Transactions, *77* (1), pp. 239-244.

[14] ASHRAE, 1997, *ASHRAE Handbook of Fundamentals*, American Society of Heating, Refrigerating and Air Conditioning Engineers, Inc., Atlanta, Georgia.

[15] Guan Y., Hosni M., Jones B.W., and Gielda T.P., 2003, "Literature review of the advances in thermal comfort modeling," ASHRAE Transactions, *109* (2), pp. 908-916.

[16] AIA, 2001, *Guidelines for Design and Construction of Hospitals and Health Care facilities*, American Institute of Architects, Washington, D.C.

[17] Woods J.E., Brayman D.T., Rasmussen R.W., Reynolds P.E., and Montag G.M., 1986, "Ventilation requirements in hospital operating rooms - Part I: Control of airborne particles," ASHRAE Transactions, *92* (2), pp. 396-426.

[18] Balaras C.A., Dascalaki E., Argiriou A.A., and Gaglia A., 2002, "HVAC Systems in indoor conditions in Hellenic hospital operating rooms," ASHRAE Transactions, *108* (2), pp. 23-38.

[19] Lewis J.R., 1993, "Operating room air distribution effectiveness," ASHRAE Transactions, *99* (2), pp. 1191-1199.

[20] Memarzadeh F., 2000, "Methodology for minimizing risk from airborne organisms in hospital isolation rooms," ASHRAE Transactions, *106* (2), pp. 731-742.

[21] Mora R., English M., and Athienitis A., 2001, "Assessment of thermal comfort during surgical operations," ASHRAE Transactions, *107* (1), pp. 52-62.

[22] Memarzadeh F. and Manning A., 2000, "Thermal comfort, uniformity, and ventilation effectiveness in patient rooms: performance assessment using ventilation indices," ASHRAE Transactions, *106* (2), pp. 748-761.

[23] Memarzadeh F. and Manning A., 2002, "Comparison of operating room ventilation systems in protection of the surgical site," ASHRAE Transactions, *108* (2), pp. 3-15.

[24] Ho S.H., Rosario L., Rahman M.M., 2004, "Predictions of relative humidity and temperature in an operating room," Proceedings of IMECE 2004: ASME International Mechanical Engineering Congress and RD&D Expo, on publishing.

72

Appendices

Appendix A: FIDAP Program for Office Room Simulation

```
/ file name: unf01.txt
TITLE
AIR FLOW in OFFICE ROOM - UNDERFLOOR AIR DISTRIBUTION

// FI-GEN
FI-GEN( ELEM = 1, POIN = 1, CURV = 1, SURF = 1, NODE = 0, MEDG = 1,
MLOO = 1, MFAC = 1, BEDG = 1, SPAV = 1, MSHE = 1, MSOL = 1, COOR = 1 )

$CNT = 1

/ Lengths in X and Y direction
$NLX = 13
DECLARE $LX[1:$NLX]
$LX[1] = 0.05
$LX[2] = 0.20
$LX[3] = 0.20
$LX[4] = 0.25
$LX[5] = 0.10
$LX[6] = 0.25
$LX[7] = 0.05
$LX[8] = 0.20
$LX[9] = 0.16
$LX[10] = 0.54
$LX[11] = 0.60
$LX[12] = 0.35
$LX[13] = 0.40


$NLY = 12
DECLARE $LY[1:$NLY]
$LY[1] = 0.50
$LY[2] = 0.10
$LY[3] = 0.10
$LY[4] = 0.10
$LY[5] = 0.15
$LY[6] = 0.05
$LY[7] = 0.35
$LY[8] = 0.05
$LY[9] = 0.35
$LY[10] = 0.95
$LY[11] = 0.50
$LY[12] = 0.40

/ Generate numbers of intervals
DECLARE $MX[1:$NLX]
DECLARE $MY[1:$NLY]
$ALPHA = 1.35
$L1 = 0.002

DO( $CNT = 1, $CNT .LE. $NLX )
$MX[$CNT] = 2*INT(1+LOG(1+($ALPHA-1)*0.5*$LX[$CNT]/$L1)/LOG($ALPHA))
ENDDO
$MX[10] = INT(1+LOG(1+($ALPHA-1)*$LX[10]/$L1)/LOG($ALPHA))
```

74

Appendix A: (Continued)

```
DO( $CNT = 1, $CNT .LE. $NLY )
$MY[$CNT] = 2*INT(1+LOG(1+($ALPHA-1)*0.5*$LY[$CNT]/$L1)/LOG($ALPHA))
ENDDO

/ Generate coordinates
$NX = 12
DECLARE $XP[1:$NX]
$XP[1] = 0
DO( $CNT = 1, $CNT .LT. $NX-1 )
$XP[$CNT+1] = $XP[$CNT] + $LX[$CNT]
ENDDO
$XP[12] = 0.10

$NY = 12
DECLARE $YP[1:$NY]
$YP[1] = 0
DO( $CNT = 1, $CNT .LT. $NY-1 )
$YP[$CNT+1] = $YP[$CNT] + $LY[$CNT]
ENDDO
$YP[12] = 1.00

// ADD POINTS

POINT( ADD, COOR )
$XP[1] $YP[1]
$XP[1] $YP[5]
$XP[1] $YP[6]
$XP[1] $YP[7]
$XP[1] $YP[8]
$XP[1] $YP[9]
$XP[1] $YP[10]
$XP[1] $YP[11]

$XP[2] $YP[5]
$XP[2] $YP[6]
$XP[2] $YP[7]
$XP[2] $YP[8]
$XP[2] $YP[9]
$XP[2] $YP[10]
$XP[2] $YP[11]

$XP[12] $YP[1]
$XP[12] $YP[2]
$XP[12] $YP[3]
$XP[12] $YP[4]

$XP[3] $YP[8]
$XP[3] $YP[11]

$XP[4] $YP[5]
$XP[4] $YP[6]
$XP[4] $YP[7]
$XP[4] $YP[8]
```

75

Appendix A: (Continued)

```
$XP[4] $YP[9]
$XP[4] $YP[10]
$XP[4] $YP[11]

$XP[5] $YP[1]
$XP[5] $YP[2]
$XP[5] $YP[3]
$XP[5] $YP[4]
$XP[5] $YP[5]
$XP[5] $YP[11]

$XP[6] $YP[3]
$XP[6] $YP[4]
$XP[6] $YP[5]
$XP[6] $YP[6]
$XP[6] $YP[7]
$XP[6] $YP[8]
$XP[6] $YP[9]
$XP[6] $YP[10]
$XP[6] $YP[11]

$XP[7] $YP[12]
$XP[7] $YP[9]
$XP[7] $YP[11]

$XP[8] $YP[1]
$XP[8] $YP[2]
$XP[8] $YP[12]
$XP[8] $YP[9]
$XP[8] $YP[10]
$XP[8] $YP[11]

$XP[9] $YP[1]
$XP[9] $YP[11]

$XP[10] $YP[1]
$XP[10] $YP[11]

$XP[11] $YP[1]
$XP[11] $YP[2]
$XP[11] $YP[12]
$XP[11] $YP[9]
$XP[11] $YP[10]
$XP[11] $YP[11]

// ADD LINES

POINT( SELE, ID)
1 8
CURVE( ADD, LINE )

POINT( SELE, ID)
9 15
```

76

Appendix A: (Continued)

```
CURVE( ADD, LINE )

POINT( SELE, ID)
16 19
CURVE( ADD, LINE )

POINT( SELE, ID)
22 28
CURVE( ADD, LINE )

POINT( SELE, ID)
29 33
CURVE( ADD, LINE )

POINT( SELE, ID)
35 43
CURVE( ADD, LINE )

POINT( SELE, ID)
44 45
CURVE( ADD, LINE )

POINT( SELE, ID)
47 52
CURVE( ADD, LINE )

POINT( SELE, ID)
57 62
CURVE( ADD, LINE )

POINT( SELE, ID)
1
16
29
47
53
55
57
CURVE( ADD, LINE )

POINT( SELE, ID)
30
48
CURVE( ADD, LINE )

POINT( SELE, ID)
31
35
CURVE( ADD, LINE )

POINT( SELE, ID)
19
32
```

77

Appendix A: (Continued)

```
CURVE( ADD, LINE )

POINT( SELE, ID)
2
9
CURVE( ADD, LINE )

POINT( SELE, ID)
22
33
37
CURVE( ADD, LINE )

POINT( SELE, ID)
10
23
CURVE( ADD, LINE )

POINT( SELE, ID)
11
24
CURVE( ADD, LINE )

POINT( SELE, ID)
44
49
CURVE( ADD, LINE )

POINT( SELE, ID)
12
20
25
CURVE( ADD, LINE )

POINT( SELE, ID)
41
45
50
CURVE( ADD, LINE )

POINT( SELE, ID)
8
15
21
28
34
43
46
52
54
56
62
CURVE( ADD, LINE )
```

Appendix A: (Continued)

```
// ADD SURFACES

POINT(SELE, ID )
8
62
1
57
SURFACE( ADD, POIN, ROWW = 2 )

// ADD MESH EDGES

CURVE( SELE, ID )
55
65
MEDGE( ADD, FRTL, INTE = $MX[1], RATI = $L1, 2RAT = $L1, PCEN = 0 )

CURVE( SELE, ID )
58
59
MEDGE( ADD, FRTL, INTE = $MX[13], RATI = $L1, 2RAT = $L1, PCEN = 0 )

CURVE( SELE, ID )
61
66
MEDGE( ADD, FRTL, INTE = $MX[2], RATI = $L1, 2RAT = $L1, PCEN = 0 )

CURVE( SELE, ID )
62
67
MEDGE( ADD, FRTL, INTE = $MX[3], RATI = $L1, 2RAT = $L1, PCEN = 0 )

CURVE( SELE, ID )
56
68
MEDGE( ADD, FRTL, INTE = $MX[4], RATI = $L1, 2RAT = $L1, PCEN = 0 )

CURVE( SELE, ID )
53
57
69
MEDGE( ADD, FRTL, INTE = $MX[5], RATI = $L1, 2RAT = $L1, PCEN = 0 )

CURVE( SELE, ID )
63
70
MEDGE( ADD, FRTL, INTE = $MX[6], RATI = $L1, 2RAT = $L1, PCEN = 0 )

CURVE( SELE, ID )
60
64
71
MEDGE( ADD, FRTL, INTE = $MX[7], RATI = $L1, 2RAT = $L1, PCEN = 0 )
```

79

Appendix A: (Continued)

```
CURVE( SELE, ID )
49
72
MEDGE( ADD, FRTL, INTE = $MX[8], RATI = $L1, 2RAT = $L1, PCEN = 0 )

CURVE( SELE, ID )
50
73
MEDGE( ADD, FRTL, INTE = $MX[9], RATI = $L1, 2RAT = $L1, PCEN = 0 )

CURVE( SELE, ID )
51
74
MEDGE( ADD, FRTL, INTE = $MX[10], RATI = $L1, 2RAT = 0, PCEN = 0 )

CURVE( SELE, ID )
47
54
MEDGE( ADD, FRTL, INTE = $MX[11], RATI = $L1, 2RAT = $L1, PCEN = 0 )

CURVE( SELE, ID )
48
52
MEDGE( ADD, FRTL, INTE = $MX[12], RATI = $L1, 2RAT = $L1, PCEN = 0 )

CURVE( SELE, ID )
14
23
36
41
MEDGE( ADD, FRTL, INTE = $MY[1], RATI = $L1, 2RAT = $L1, PCEN = 0 )

CURVE( SELE, ID )
15
24
MEDGE( ADD, FRTL, INTE = $MY[2], RATI = $L1, 2RAT = $L1, PCEN = 0 )

CURVE( SELE, ID )
16
25
27
MEDGE( ADD, FRTL, INTE = $MY[3], RATI = $L1, 2RAT = $L1, PCEN = 0 )

CURVE( SELE, ID )
26
28
MEDGE( ADD, FRTL, INTE = $MY[4], RATI = $L1, 2RAT = $L1, PCEN = 0 )

CURVE( SELE, ID )
2
8
17
29
```

80

Appendix A: (Continued)

```
MEDGE( ADD, FRTL, INTE = $MY[5], RATI = $L1, 2RAT = $L1, PCEN = 0 )

CURVE( SELE, ID )
3
9
18
30
MEDGE( ADD, FRTL, INTE = $MY[6], RATI = $L1, 2RAT = $L1, PCEN = 0 )

CURVE( SELE, ID )
4
10
19
31
MEDGE( ADD, FRTL, INTE = $MY[7], RATI = $L1, 2RAT = $L1, PCEN = 0 )

CURVE( SELE, ID )
5
11
20
32
MEDGE( ADD, FRTL, INTE = $MY[8], RATI = $L1, 2RAT = $L1, PCEN = 0 )

CURVE( SELE, ID )
6
12
21
33
39
44
MEDGE( ADD, FRTL, INTE = $MY[9], RATI = $L1, 2RAT = $L1, PCEN = 0 )

CURVE( SELE, ID )
7
13
22
34
40
45
MEDGE( ADD, FRTL, INTE = $MY[10], RATI = $L1, 2RAT = $L1, PCEN = 0 )

CURVE( SELE, ID )
37
42
MEDGE( ADD, FRTL, INTE = $MY[11], RATI = $L1, 2RAT = $L1, PCEN = 0 )

CURVE( SELE, ID )
35
38
43
MEDGE( ADD, FRTL, INTE = $MY[12], RATI = $L1, 2RAT = $L1, PCEN = 0 )

// ADD MESH LOOPS
```

81

Appendix A: (Continued)

```
CURVE( SELE, ID )
55
2 7
65
13
12
11
10
9
8
MLOOP( ADD, MAP, EDG1 = 1, EDG2 = 6, EDG3 = 1, EDG4 = 6 )

CURVE( SELE, ID )
58
9
59
18
MLOOP( ADD, MAP, EDG1 = 1, EDG2 = 1, EDG3 = 1, EDG4 = 1 )

CURVE( SELE, ID )
62
61
11 13
66 67
22
21
20
MLOOP( ADD, MAP, EDG1 = 2, EDG2 = 3, EDG3 = 2, EDG4 = 3 )

CURVE( SELE, ID )
57
56
17 22
68 69
34
33
32
31
30
29
MLOOP( ADD, MAP, EDG1 = 2, EDG2 = 6, EDG3 = 2, EDG4 = 6 )

CURVE( SELE, ID )
53
25 26
57
28
27
MLOOP( ADD, MAP, EDG1 = 1, EDG2 = 2, EDG3 = 1, EDG4 = 2 )

CURVE( SELE, ID )
64
63
```

82

Appendix A: (Continued)

```
33 34
70 71
40
39
MLOOP( ADD, MAP, EDG1 = 2, EDG2 = 2, EDG3 = 2, EDG4 = 2 )

CURVE( SELE, ID )
60
35
64
38
MLOOP( ADD, MAP, EDG1 = 1, EDG2 = 1, EDG3 = 1, EDG4 = 1 )

CURVE( SELE, ID )
47
14 16
54
25
24
23
MLOOP( ADD, MAP, EDG1 = 1, EDG2 = 3, EDG3 = 1, EDG4 = 3 )

CURVE( SELE, ID )
48
23
52
36
MLOOP( ADD, MAP, EDG1 = 1, EDG2 = 1, EDG3 = 1, EDG4 = 1 )

CURVE( SELE, ID )
51
50
49
36 40
72 74
45
44
43
42
41
MLOOP( ADD, MAP, EDG1 = 3, EDG2 = 5, EDG3 = 3, EDG4 = 5 )

// ADD MESH FACES

DO( $CNT = 1, $CNT .LE. 10 )
SURFACE( SELE, ID = 1 )
MLOOP( SELE, ID = $CNT )
MFACE( ADD )
ENDDO

// GENERATE MESH

MFACE( SELE, ALL )
```

83

Appendix A: (Continued)

```
MFACE( MESH, MAP, ENTI = "air" )

// BOUNDARY ENTITIES

ELEMENT( SETD, EDGE, NODE = 2 )

MEDGE( SELE, ID = 24 )
MEDGE( MESH, MAP, ENTI = "outlet" )

MEDGE( SELE, ID = 21 )
MEDGE( MESH, MAP, ENTI = "inlet" )

MEDGE( SELE, ID )
62
32
69
72
61
67
MEDGE( MESH, MAP, ENTI = "symmetry" )

MEDGE( SELE, ID )
/ceiling
2
8
10
22
6
/lights
13
15
18
20
/floor
25
27
19
23
/person
11
37
39
43
47
51
55
14
70
/chair
16
68
28
34
```

84

Appendix A: (Continued)

```
/desk
29
33
35
26
38
9
1
/computer
41 42
3 4
49 50
5
7
/panel
40
44
48
52
56
MEDGE( MESH, MAP, ENTI = "nonslip" )

MEDGE( SELE, ID )
11
37
39
43
47
51
55
14
70
MEDGE( MESH, MAP, ENTI = "person" )

MEDGE( SELE, ID )
5
7
MEDGE( MESH, MAP, ENTI = "hottop" )

MEDGE( SELE, ID )
13
15
18
20
MEDGE( MESH, MAP, ENTI = "lights" )

MEDGE( SELE, ID )
25
27
19
23
MEDGE( MESH, MAP, ENTI = "floor" )
END
```

85

Appendix A: (Continued)

```
FIPREP

/ SI units
/ Reference temperature: 22 oC = 295 K
/ Underfloor air distribution: $U2 m/s

$U2 = 1

DENSITY( CONS = 1.1967 )
VISCOSITY( CONS = 1.8273E-5 )
SPECIFICHEAT( CONS = 1.0043E3 )
CONDUCTIVITY( CONS = 2.5776E-2 )
VOLUMEX( CONS = 3.3932E-3, REFTEMP = 22 )
GRAVITY( MAGNITUDE = 9.8 )
DIFFUSIVITY( SET = "H2O", CONS = 2.5448E-5 )
DIFFUSIVITY( SET = "NH3", CONS = 2.5033E-5 )

ENTITY( FLUI, NAME = "air", SPEC = 1, MDIFF = "H2O", SPEC = 2, MDIFF =
"NH3" )
ENTITY( PLOT, NAME = "outlet" )
ENTITY( PLOT, NAME = "inlet" )
ENTITY( PLOT, NAME = "symmetry" )
ENTITY( PLOT, NAME = "nonslip" )
ENTITY( PLOT, NAME = "person" )
ENTITY( PLOT, NAME = "hottop" )
ENTITY( PLOT, NAME = "lights" )
ENTITY( PLOT, NAME = "floor" )

BCNODE( VELO, ENTI = "inlet", CONS, X = 0, Y = $U2 )
BCNODE( VELO, ENTI = "nonslip", ZERO )
BCNODE( UX, ENTI = "symmetry", ZERO )

BCNODE( TEMP, ENTI = "inlet", CONS = 20 )
BCNODE( TEMP, ENTI = "person", CONS = 33 )
BCFLUX( HEAT, ENTI = "hottop", CONS = 100 )
BCFLUX( HEAT, ENTI = "lights", CONS = 75 )

BCNODE( SPEC = 1, ENTI = "inlet", CONS = 0.011 )
BCFLUX( SPEC = 1, ENTI = "person", CONS = 5E-7 )

BCNODE( SPEC = 2, ENTI = "inlet", CONS = 0 )
BCFLUX( SPEC = 2, ENTI = "floor", CONS = 1E-6 )

CLIPPING( MINI )
0 0 0 0 20 0 0 0 1.E-20 1.E-20
CLIPPING( MAXI )
0 0 0 0 0 0 0 0 1. 1.

RENUMBER( PROFILE )
DATAPRINT( NONE )
PRINTOUT( NONE, NOBO )
OPTIONS( UPWI )
EXECUTION( NEWJ )
```

86

Appendix A: (Continued)

```
PRESSURE( PENA = 1.E-7, DISC )
PROBLEM( 2-D, NONL, MOME, BUOY )
SOLUTION( S.S. = 1000, VELC = 0.02, RESC = 0.02, ACCF = 0.5 )

/ICNODE( VELO, READ, ALL )
/EXECUTION( NEWJ )
/PROBLEM( 2-D, NONL, NOMO, SPEC = 1, SPEC = 2 )

END

CREATE( FISOLV )
RUN( FISOLV, IDENT = "unf01a", BACK )
/RUN( FISOLV, IDENT = "unf01z", REST = "unf01a.FDPOST", BACK )
```

Appendix B: FIDAP Program for Operating Room Simulation

```
/ Input file for mixed convection in OR, SI units
/ file name: 3500.txt
/ basic configuration, single outlet OL = 35, angle 0 deg.

TITLE
AIRFLOW in O.R. - Simulation No. SI-35-00

// FI-GEN
FI-GEN( ELEM = 1, POIN = 1, CURV = 1, SURF = 1, NODE = 0, MEDG = 1,
MLOO = 1, MFAC = 1, BEDG = 1, SPAV = 1, MSHE = 1, MSOL = 1, COOR = 1 )

$NX = 10
DECLARE $X_VALS[1:$NX]
$X_VALS[1] = 0
$X_VALS[2] = 1.75
$X_VALS[3] = 2.00
$X_VALS[4] = 2.10
$X_VALS[5] = 2.70
$X_VALS[6] = 3.30
$X_VALS[7] = 3.90
$X_VALS[8] = 4.00
$X_VALS[9] = 4.25
$X_VALS[10] = 6.00

$NY = 11
DECLARE $Y_VALS[1:$NY]
$Y_VALS[1] = 3.50
$Y_VALS[2] = 3.20
$Y_VALs[3] = 3.00
$Y_VALS[4] = 2.85
$Y_VALS[5] = 2.55
$Y_VALS[6] = 1.75
$Y_VALS[7] = 1.05
$Y_VALS[8] = 0.80
$Y_VALS[9] = 0.55
$Y_VALS[10] = 0.20
$Y_VALS[11] = 0

$NL = 18
DECLARE $LEN[1:$NL]
DECLARE $MSH[1:$NL]
$LEN[1] = 1.75
$LEN[2] = 0.25
$LEN[3] = 0.10
$LEN[4] = 0.60
$LEN[5] = 0.60
$LEN[6] = 1.80
$LEN[7] = 0.30
$LEN[8] = 0.20
$LEN[9] = 0.15
$LEN[10] = 0.30
$LEN[11] = 0.80
$LEN[12] = 1.55
```

88

Appendix B: (Continued)

```
$LEN[13] = 0.20
$LEN[14] = 0.70
$LEN[15] = 0.25
$LEN[16] = 0.60
$LEN[17] = 1.20
$LEN[18] = 0.35


$ALPHA = 1.1
$L1 = 0.01

DO( $I = 1, $I .LE. $NL )
$MSH[$I] = 2*INT(1+LOG(1+($ALPHA-1)*0.5*$LEN[$I]/$L1)/LOG($ALPHA))
ENDDO

// Add Points

//1st row
$Y_VAL = $Y_VALS[1]
DO( $I = 1, $I .LE. $NX )
POINT( ADD, COOR, X = $X_VALS[$I], Y = $Y_VAL )
ENDDO

//2nd row
$Y_VAL = $Y_VALS[2]
POINT( ADD, COOR, X = $X_VALS[1], Y = $Y_VAL )
POINT( ADD, COOR, X = $X_VALS[$NX], Y = $Y_VAL )

//3rd row
$Y_VAL = $Y_VALS[3]
POINT( ADD, COOR, X = $X_VALS[1], Y = $Y_VAL )
POINT( ADD, COOR, X = $X_VALS[$NX], Y = $Y_VAL )

//4th row
$Y_VAL = $Y_VALS[4]
DO( $I = 1, $I .LE. $NX )
POINT( ADD, COOR, X = $X_VALS[$I], Y = $Y_VAL )
ENDDO

//5th row
$Y_VAL = $Y_VALS[5]
DO( $I = 1, $I .LE. $NX )
POINT( ADD, COOR, X = $X_VALS[$I], Y = $Y_VAL )
ENDDO

//6th row
$Y_VAL = $Y_VALS[6]
DO( $I = 1, $I .LE. $NX )
POINT( ADD, COOR, X = $X_VALS[$I], Y = $Y_VAL )
ENDDO

//7th row
$Y_VAL = $Y_VALS[7]
DO( $I = 3, $I .LE. 8 )
```

89

Appendix B: (Continued)

```
POINT( ADD, COOR, X = $X_VALS[$I], Y = $Y_VAL )
ENDDO

//8th row
$Y_VAL = $Y_VALS[8]
POINT( ADD, COOR, X = $X_VALS[3], Y = $Y_VAL )
POINT( ADD, COOR, X = $X_VALS[4], Y = $Y_VAL )
POINT( ADD, COOR, X = $X_VALS[7], Y = $Y_VAL )
POINT( ADD, COOR, X = $X_VALS[8], Y = $Y_VAL )

//9th row
$Y_VAL = $Y_VALS[9]
POINT( ADD, COOR, X = $X_VALS[9], Y = $Y_VAL )
POINT( ADD, COOR, X = $X_VALS[10], Y = $Y_VAL )

//10th row
$Y_VAL = $Y_VALS[10]
DO( $I = 1, $I .LE. 4 )
POINT( ADD, COOR, X = $X_VALS[$I], Y = $Y_VAL )
ENDDO
DO( $I = 7, $I .LE. 10 )
POINT( ADD, COOR, X = $X_VALS[$I], Y = $Y_VAL )
ENDDO

//11th row
$Y_VAL = $Y_VALS[11]
DO( $I = 1, $I .LE. 4 )
POINT( ADD, COOR, X = $X_VALS[$I], Y = $Y_VAL )
ENDDO
DO( $I = 7, $I .LE. 10 )
POINT( ADD, COOR, X = $X_VALS[$I], Y = $Y_VAL )
ENDDO

// Add Lines

POINT( SELE, ID)
1 10
CURVE( ADD, LINE )

POINT( SELE, ID)
15 24
CURVE( ADD, LINE )

POINT( SELE, ID)
25 34
CURVE( ADD, LINE )
POINT( SELE, ID)
35 44
CURVE( ADD, LINE )

POINT( SELE, ID)
45 50
CURVE( ADD, LINE )
```

90

Appendix B: (Continued)

```
POINT( SELE, ID)
51 54
CURVE( ADD, LINE )

POINT( SELE, ID)
57 64
CURVE( ADD, LINE )

POINT( SELE, ID)
65 72
CURVE( ADD, LINE )

POINT( SELE, ID)
1
11
13
15
25
35
57
65
CURVE( ADD, LINE )

POINT( SELE, ID)
10
12
14
24
34
44
56
64
72
CURVE( ADD, LINE )

POINT( SELE, ID)
19
29
CURVE( ADD, LINE )
POINT( SELE, ID)
20
30
CURVE( ADD, LINE )

POINT( SELE, ID)
46
52
CURVE( ADD, LINE )
POINT( SELE, ID)
49
53
CURVE( ADD, LINE )
```

91

Appendix B: (Continued)

```
POINT( SELE, ID)
37
45
51
59
CURVE( ADD, LINE )

POINT( SELE, ID)
42
50
54
62
CURVE( ADD, LINE )

POINT( SELE, ID)
36
58
CURVE( ADD, LINE )
POINT( SELE, ID)
43
55
63
CURVE( ADD, LINE )

//Add Surfaces

POINT(SELE, ID )
1
10
65
72
SURFACE( ADD, POIN, ROWW = 2 )

//Add Mesh Edges

CURVE( SELE, ID )
1
10
19
28
45
52
9
18
27
36
51
58
MEDGE( ADD, FRTL, INTE = $MSH[1], RATI = $L1, 2RAT = $L1, PCEN = 0 )

CURVE( SELE, ID )
2
11
```

92

Appendix B: (Continued)

```
20
29
46
53
8
17
26
35
50
57
MEDGE( ADD, FRTL, INTE = $MSH[2], RATI = $L1, 2RAT = $L1, PCEN = 0 )

CURVE( SELE, ID )
3
12
21
30
37
42
47
54
7
16
25
34
41
44
49
56
MEDGE( ADD, FRTL, INTE = $MSH[3], RATI = $L1, 2RAT = $L1, PCEN = 0 )

CURVE( SELE, ID )
4
13
22
31
38
MEDGE( ADD, FRTL, INTE = $MSH[4], RATI = $L1, 2RAT = $L1, PCEN = 0 )

CURVE( SELE, ID )
6
15
24
33
40
MEDGE( ADD, FRTL, INTE = $MSH[4], RATI = $L1, 2RAT = $L1, PCEN = 0 )

CURVE( SELE, ID )
5
14
23
32
39
```

93

Appendix B: (Continued)

```
MEDGE( ADD, FRTL, INTE = $MSH[5], RATI = $L1, 2RAT = $L1, PCEN = 0 )

CURVE( SELE, ID )
43
48
55
MEDGE( ADD, FRTL, INTE = $MSH[6], RATI = $L1, 2RAT = $L1, PCEN = 0 )

CURVE( SELE, ID )
59
66
MEDGE( ADD, FRTL, INTE = $MSH[7], RATI = $L1, 2RAT = $L1, PCEN = 0 )

CURVE( SELE, ID )
60
67
MEDGE( ADD, FRTL, INTE = $MSH[8], RATI = $L1, 2RAT = $L1, PCEN = 0 )

CURVE( SELE, ID )
61
68
MEDGE( ADD, FRTL, INTE = $MSH[9], RATI = $L1, 2RAT = $L1, PCEN = 0 )

CURVE( SELE, ID )
62
74
75
69
MEDGE( ADD, FRTL, INTE = $MSH[10], RATI = $L1, 2RAT = $L1, PCEN = 0 )

CURVE( SELE, ID )
63
70
MEDGE( ADD, FRTL, INTE = $MSH[11], RATI = $L1, 2RAT = $L1, PCEN = 0 )

CURVE( SELE, ID )
64
84
MEDGE( ADD, FRTL, INTE = $MSH[12], RATI = $L1, 2RAT = $L1, PCEN = 0 )

CURVE( SELE, ID )
65
73
MEDGE( ADD, FRTL, INTE = $MSH[13], RATI = $L1, 2RAT = $L1, PCEN = 0 )

CURVE( SELE, ID )
78
81
MEDGE( ADD, FRTL, INTE = $MSH[14], RATI = $L1, 2RAT = $L1, PCEN = 0 )

CURVE( SELE, ID )
79
76
```

94

Appendix B: (Continued)

```
77
82
MEDGE( ADD, FRTL, INTE = $MSH[15], RATI = $L1, 2RAT = $L1, PCEN = 0 )

CURVE( SELE, ID )
80
83
MEDGE( ADD, FRTL, INTE = $MSH[16], RATI = $L1, 2RAT = $L1, PCEN = 0 )

CURVE( SELE, ID )
85
71
MEDGE( ADD, FRTL, INTE = $MSH[17], RATI = $L1, 2RAT = $L1, PCEN = 0 )

CURVE( SELE, ID )
86
72
MEDGE( ADD, FRTL, INTE = $MSH[18], RATI = $L1, 2RAT = $L1, PCEN = 0 )

//Add Mesh Loops

CURVE( SELE, ID )
61
60
59
1 9
66 68
18
17
16
15
14
13
12
11
10
MLOOP( ADD, MAP, EDG1 = 3, EDG2 = 9, EDG3 = 3, EDG4 = 9 )

CURVE( SELE, ID )
62
10 13
74
22
21
20
19
MLOOP( ADD, MAP, EDG1 = 1, EDG2 = 4, EDG3 = 1, EDG4 = 4 )

CURVE( SELE, ID )
75
15 18
69
27
```

95

Appendix B: (Continued)

```
26
25
24
MLOOP( ADD, MAP, EDG1 = 1, EDG2 = 4, EDG3 = 1, EDG4 = 4 )

CURVE( SELE, ID )
63
19 27
70
36
35
34
33
32
31
30
29
28
MLOOP( ADD, MAP, EDG1 = 1, EDG2 = 9, EDG3 = 1, EDG4 = 9 )

CURVE( SELE, ID )
65
45 51
73
58
57
56
55
54
53
52
MLOOP( ADD, MAP, EDG1 = 1, EDG2 = 7, EDG3 = 1, EDG4 = 7 )

CURVE( SELE, ID )
64
28
84
45
MLOOP( ADD, MAP, EDG1 = 1, EDG2 = 1, EDG3 = 1, EDG4 = 1 )

CURVE( SELE, ID )
86
85
36
71 72
51
MLOOP( ADD, MAP, EDG1 = 2, EDG2 = 1, EDG3 = 2, EDG4 = 1 )

CURVE( SELE, ID )
78
30 34
81
41
```

96

Appendix B: (Continued)

```
40
39
38
37
MLOOP( ADD, MAP, EDG1 = 1, EDG2 = 5, EDG3 = 1, EDG4 = 5 )

CURVE( SELE, ID )
80
42 44
83
49
48
47
MLOOP( ADD, MAP, EDG1 = 1, EDG2 = 3, EDG3 = 1, EDG4 = 3 )

CURVE( SELE, ID )
79
37
76
42
MLOOP( ADD, MAP, EDG1 = 1, EDG2 = 1, EDG3 = 1, EDG4 = 1 )

CURVE( SELE, ID )
77
41
82
44
MLOOP( ADD, MAP, EDG1 = 1, EDG2 = 1, EDG3 = 1, EDG4 = 1 )

//Add Mesh Faces
DO( $I = 1, $I .LE. 11 )
SURFACE( SELE, ID = 1 )
MLOOP( SELE, ID = $I )
MFACE( ADD )
ENDDO

//Meshing Mesh Faces
ELEMENT( SETD, QUAD, NODE = 4 )
MFACE( SELE, ALL )
MFACE( MESH, MAP, ENTI = "air" )

//Mesh Map (Boundary Entities )
ELEMENT( SETD, EDGE, NODE = 2 )
MEDGE( SELE, ID )
   61
   63
MEDGE( MESH, MAP, ENTI = "inlet" )
MEDGE( SELE, ID )
   86
MEDGE( MESH, MAP, ENTI = "outlet" )
MEDGE( SELE, ID )
/ walls
   59,    60
```

97

Appendix B: (Continued)

```
   62
   64,    65
   68,    71
   84
   73,    74
/ ceiling
    1
   13
   25
   41
   51
   46
   33
   19
    7
/ floor
    6
   18
   32
   58
   40
   24
   12
/ surgical lights
   66,    67
   52,    53
/ patient + table
   78,    79
   45
   55,    56
   50
/ staffs
   16,    17
   72
   75
   77
   81
   22,    23
   76
   80
   82,    83
   85
MEDGE( MESH, MAP, ENTI = "nonslip" )
MEDGE( SELE, ID )
   59,    60
   62
   64,    65
   68,    71
   84
   73,    74
MEDGE( MESH, MAP, ENTI = "walls" )
MEDGE( SELE, ID )
   66,    67
```

98

Appendix B: (Continued)

```
    52
MEDGE( MESH, MAP, ENTI = "lamp_back" )
MEDGE( SELE, ID )
    53
MEDGE( MESH, MAP, ENTI = "lamp_face" )
MEDGE( SELE, ID )
    78,    79
    45
    55
    50
MEDGE( MESH, MAP, ENTI = "patient" )
MEDGE( SELE, ID )
    16,    17
    72
    75
    77
    81
    22,    23
    76
    80
    82,    83
    85
MEDGE( MESH, MAP, ENTI = "staffs" )

END

FIPREP

$Un = 0.4
$Ang = 0

DENSITY( CONS = 1.1967 )
VISCOSITY( CONS = 1.8273e-05 )
SPECIFICHEAT( CONS = 1004.3 )
CONDUCTIVITY( CONS = 0.025776 )
VOLUMEXPANSION( CONS = 0.0033932, REFT = 22 )
GRAVITY( MAGN = 9.80665 )
DIFFUSIVITY( SET = "H2O", CONS = 2.5448e-05 )
DIFFUSIVITY( SET = "NH3", CONS = 2.5033e-05 )

ENTITY( FLUI, NAME = "air", SPEC = 1, MDIF = "H2O", SPEC = 2, MDIF =
"NH3" )
ENTITY( PLOT, NAME = "outlet" )
ENTITY( PLOT, NAME = "inlet" )
ENTITY( PLOT, NAME = "nonslip" )
ENTITY( PLOT, NAME = "walls" )
ENTITY( PLOT, NAME = "lamp_back" )
ENTITY( PLOT, NAME = "lamp_face" )
ENTITY( PLOT, NAME = "patient" )
ENTITY( PLOT, NAME = "staffs" )

BCNODE( VELO, ENTI = "inlet", CONS, X = $Un*COS($Ang), Y = -
$Un*SIN($Ang) )
```

99

Appendix B: (Continued)

```
BCNODE( VELO, ENTI = "nonslip", ZERO )

BCNODE( TEMP, ENTI = "inlet", CONS = 17 )
BCNODE( TEMP, ENTI = "walls", CONS = 22 )
BCNODE( TEMP, ENTI = "patient", CONS = 33 )
BCNODE( TEMP, ENTI = "staffs", CONS = 33 )
BCFLUX( HEAT, ENTI = "lamp_back", CONS = 5 )
BCFLUX( HEAT, ENTI = "lamp_face", CONS = 100 )

BCNODE( SPEC = 1, ENTI = "inlet", CONS = 0.01018 )
BCFLUX( SPEC = 1, ENTI = "patient", CONS = 5e-07 )
BCFLUX( SPEC = 1, ENTI = "staffs", CONS = 8e-07 )

BCNODE( SPEC = 2, ENTI = "inlet", CONS = 0 )
BCFLUX( SPEC = 2, ENTI = "patient", CONS = 1e-05 )

CLIPPING( MINI )
0 0 0 0 17 0 0 0 1.E-20 1.E-20
CLIPPING( MAXI )
0 0 0 0 0 0 0 0 1. 1.

DATAPRINT( NONE )
PRINTOUT( NONE )
OPTIONS( UPWI )
EXECUTION( NEWJ )

PRESSURE( PENA = 1e-07, DISC )
PROBLEM( 2-D, NONL, MOME, BUOY )
SOLUTION( S.S. = 1000, VELC = 0.02, RESC = 0.02, ACCF = 0.5 )

/ICNODE( VELO, READ, ALL )
/EXECUTION( NEWJ )
/PROBLEM( 2-D, NONL, NOMO, SPEC = 1, SPEC = 2 )

END

CREATE( FISO )
RUN( FISOLV, IDENT = "3500a", BACK )
/RUN( FISOLV, IDENT = "3500z", REST = "3500a.FDPOST", BACK )
```

100